Eur. Phys. J. Plus (2020) 135:198
https://doi.org/10.1140/epjp/s13360-020-00121-4

THE EUROPEAN PHYSICAL JOURNAL PLUS

Regular Article

On the modeling of a solar, wind and fossil fuel energy source by means of the thermostatted kinetic theory

Marco Dalla Via[1,a], **Carlo Bianca**[1,b], **Ikram El Abbassi**[2,c], **Abdelmoumen Darcherif**[1,d]

[1] Laboratoire QUARTZ EA 7393 and Laboratoire de Recherche en Eco-innovation Industrielle et Énergétique, École Supérieure d'Ingénieurs en Génie Électrique, Productique et Management Industriel, Cergy Pontoise Cedex, France

[2] Laboratoire de Recherche en Eco-innovation Industrielle et Énergétique, École Supérieure d'Ingénieurs en Génie Électrique, Productique et Management Industriel, Cergy Pontoise Cedex, France

Received: 4 October 2019 / Accepted: 5 December 2019
© Società Italiana di Fisica (SIF) and Springer-Verlag GmbH Germany, part of Springer Nature 2020

Abstract This paper is devoted to the modeling of a hybrid energy distribution network with storage, within the thermostatted kinetic theory framework. The network consists of a non-renewable energy source and a renewable energy source. The energy storage is modeled by the introduction of the external force field coupled to the thermostat term. The activation parameters of the energy sources are assumed time-dependent in order to mimic the time-dependent efficiency of different specific energy sources. In particular a solar energy source, a wind energy source and a fossil fuel energy source are modeled. A computational analysis is performed to show the effects of the intermittent activation on the plan of quality improvement of the energy provided to the customers and on the construction of the energy storage. Discussions and future research perspectives are proposed in the last section of the paper.

1 Introduction

The transition towards a greater employment of the renewable resources is one of the most important challenges of the modern era [1–4] and attracts researchers from different domains. The integration of the renewable energy sources into the existing energy distribution systems is the first step of this process [5,6] and requires a careful analysis of the specificity of the different energy sources. In particular, the intermittency and the stochastic nature of the renewable energy must be taken into account [7,8] while the economic affordability of the fossil fuel can play a key-role in the management of the non-renewable energy sources [9].

The approaches for the design and modeling of a hybrid energy multisource network take advantage of different mathematical tools such as ODE [10,11], complex networks [12,13], optimization methods [14,15] (the interested reader is referred to [16] for a recent review). The modeling interest focuses on the development of a smart grid [17–19] where the energy

[a] e-mail: m.dallavia@ecam-epmi.com
[b] e-mail: c.bianca@ecam-epmi.com
[c] e-mail: i.elabbassi@ecam-epmi.com
[d] e-mail: m.darcherif@ecam-epmi.com

Published online: 03 February 2020

sources are able to communicate and cooperate in order to ensure the energy supply to the customers. Moreover, the employment of energy storages allows to cope with the intermittent efficiency of the renewable energy sources [20,21].

Recently, the complex character of the energy network [22,23] has suggested the employment of the thermostatted kinetic theory for the modeling of a hybrid multisource energy network with storage, see [24]. The modeling of complex systems by means of the thermostatted kinetic theory [25] has already proved to be effective when applied to biology [26,27] and to the pedestrian dynamics [28]. This approach is addressed to the modeling of complex systems whose particles are able to express a strategy (activity) and are grouped into different functional subsystems. Each functional subsystem is described by means of a distribution function over the microscopic state of the particles and the moments of the distribution functions represent the macroscopic quantities such as the density and the energy. The time evolution of the functional subsystems is driven by the mutual interactions among them and is described by means of a nonlinear integro-differential equations system. The modeling of a macroscopic action on the system is performed by introducing an external force field acting on each functional subsystem. Analogously to the molecular dynamics simulations [29,30], the force field is coupled to a damping term, the thermostat term, in order to control the global activation energy of the system and allow the existence of nonequilibrium stationary states. The reader interested in more details concerning the thermostat is addressed to the paper [31] and to the recent review [32].

According to the thermostatted kinetic theory framework proposed in [24], each energy source of the network is modeled as a functional subsystem. The representation of the energy source is performed by means of a distribution function over the environmental quality parameter and a continuous variable modeling the energy value produced by the energy source. The interest is also addressed to the construction of the energy storage which is mimicked by introducing the external force field coupled to the thermostat.

The present paper deals with the derivation and the analysis of a specific model within the paradigm proposed in [24]. In particular the modeling interest focuses on a network composed of a non-renewable and a renewable energy source. The interactions are modeled according to the stochastic games theory [33] that determines the activation of the sources and the increase in the heterogeneity of the produced energy values. The paper [34] has investigated the role of the parameters in the planning of quality improvement of the energy provided to the customers and the effect of the magnitude of the external force field on the construction of the storage system.

The novelty proposed in the present paper concerns the introduction of time-dependent parameters for the activation of the energy sources. Indeed the modeling interest takes into account the aformentioned specificity of the energy sources whose efficiency can change considerably over time. In particular three different energy sources are considered and modeled separately: a solar energy source, affected by the day-night cycle, a wind energy source, affected by the speed of the wind and a non-renewable fossil fuel energy source, affected by the fossil fuel price. Numerical simulations are performed in order to analyze, on the one hand, the effects of the time-dependent activation of the energy sources on the plan of quality improvement of the energy provided to the customers and, on the other hand, the influence on the construction of the energy storage. The computational analysis shows that the intermittency and stochastic nature of the renewable energy sources can affect the quality of the energy provided to the customers, as well as the fossil fuel price-driven management of the network. For what concerns the energy storage, the time-dependent activation of the energy sources does not affect the allocation of the energy into the storage.

This paper is organized into five more sections, which follow this introduction, and an appendix. Section 2 is concerned with the presentation of the mathematical model for the network of two energy sources derived within the thermostatted kinetic theory framework, and with the sketch of the computational analysis interest. Section 3 is devoted to the modeling of a solar energy source. Section 4 is devoted to the modeling of a wind energy source. Section 5 is devoted to the modeling of a fossil fuel energy source. Discussions and further research perspectives are postponed to Sect. 6. Finally, the Appendix provides more details about the hybrid thermostatted kinetic theory framework for the modeling of a network composed of two energy sources.

2 The mathematical model

This section is devoted to the presentation of the mathematical model analyzed in the present paper and derived within the general paradigm proposed in [24] (see the Appendix A for more details, where $F_1 = F_2 = F$). Specifically a network composed of a non-renewable energy source NR, a renewable energy source R and an energy storage is considered. The overall system is described by a distribution function vector $\mathbf{f} = (f_1(t, w), f_2(t, w))$ where $w \in D_w \subset \mathbb{R}^+$ denotes the continuous energy variable. The energy storage is taken into account by introducing a positive external force field $\mathbf{F} = (F, F) \in \left(\mathbb{R}^+\right)^2$.
The mathematical model reads as follows:

$$
\begin{aligned}
&\partial_t f_1(t,w) + F\,\partial_w\left(\left(1-\alpha_{(2,2)}[\mathbf{f}](t)\,w\right) f_1(t,w)\right)\\
&= \epsilon_{11}(t)\,(\alpha+\beta)\; f_1(t,w)\int_{D_w} f_1(t,w^*)\,\mathrm{d}w^*\\
&\quad + \epsilon_{12}(t)\,\alpha\; f_1(t,w+\lambda_1)\int_{D_w} f_2(t,w^*)\,\mathrm{d}w^*\\
&\quad + (1-\epsilon_{21}(t))\;\alpha\; f_2(t,w-\lambda_2)\int_{D_w} f_1(t,w^*)\,\mathrm{d}w^*\\
&\quad + (1-\epsilon_{22}(t))\,(\alpha+\beta)\; f_2(t,w)\int_{D_w} f_2(t,w^*)\,\mathrm{d}w^*\\
&\quad - f_1(t,w)\int_{D_w}\left((\alpha+\beta)\; f_1(t,w^*) + \alpha f_2(t,w^*)\right)\mathrm{d}w^*,\\
&\partial_t f_2(t,w) + F\,\partial_w\left(\left(1-\alpha_{(2,2)}[\mathbf{f}](t)\,w\right) f_2(t,w)\right)\\
&= (1-\epsilon_{11}(t))\,(\alpha+\beta)\; f_1(t,w)\int_{D_w} f_1(t,w^*)\,\mathrm{d}w^*\\
&\quad + (1-\epsilon_{12}(t))\;\alpha\; f_1(t,w+\lambda_1)\int_{D_w} f_2(t,w^*)\,\mathrm{d}w^*\\
&\quad + \epsilon_{21}(t)\,\alpha\; f_2(t,w-\lambda_2)\int_{D_w} f_1(t,w^*)\,\mathrm{d}w^*\\
&\quad + \epsilon_{22}(t)\,(\alpha+\beta)\; f_2(t,w)\int_{D_w} f_2(t,w^*)\,\mathrm{d}w^*\\
&\quad - f_2(t,w)\int_{D_w}\left(\alpha\; f_1(t,w^*) + (\alpha+\beta)\; f_2(t,w^*)\right)\mathrm{d}w^*,
\end{aligned}
\tag{1}
$$

where

1. $\alpha_{(2,2)}[\mathbf{f}](t)$ denotes the thermostat term which writes as follows:

$$\alpha_{(2,2)}[\mathbf{f}](t) = \frac{\sum_{j=1}^{2} u_j^2 \int_{D_w} w\, f_j(t,w)\,\mathrm{d}w}{\sum_{j=1}^{2} u_j^2 \int_{D_w} w^2\, f_j(t,w)\,\mathrm{d}w}. \tag{2}$$

2. The parameter α denotes the interaction rate between the two different energy sources, while $\alpha + \beta$, for $\alpha, \beta \in \mathbb{R}^+$, denotes the autointeraction rate.
3. The function $\epsilon_{lj}(t) : [0, +\infty[\to [0, 1]$, for $l, j \in \{1, 2\}$, denotes the activation parameter of the l-th energy source after the interaction between the l-th and j-th energy sources.
4. The parameters $\lambda_1, \lambda_2 \in [0, 1]$ denote the heterogeneity parameters of the energy source NR and of the energy source R, respectively.
5. The quantity:

$$\mathbb{E}^{[\mathbf{F}]}_{(0,0)}[f_i](t) = \int_{D_w} f_i(t,w)\,\mathrm{d}w, \quad \forall\, i \in \{1,2\}, \tag{3}$$

represents the number of customers served with the energy produced by the i-th energy source.

The activation parameters $\epsilon_{lj}(t)$, for $l, j \in \{1, 2\}$, are assumed time-dependent in order to take into account the specificity of the different energy sources and thus natural phenomena, economical aspects and technological issues.

After setting a specific initial condition $\mathbf{f}^0 = \left(f_1^0(w), f_2^0(w)\right)$, the mathematical model (1) is a nonlinear integro-differential equations system depending on 10 phenomenological parameters. From a mathematical viewpoint, the proof of the existence and uniqueness of the solution of the related initial boundary value problem is given in [24] thus allowing the possibility of employing appropriate computational methods in order to perform numerical simulations of the model. The computational model is obtained by employing the Fejér quadrature method [35] to transform the nonlinear integro-differential system (1) into an ODE system which is solved by means of a Runge–Kutta method of order 4 (MATLAB).

The numerical analysis refers to the time evolution of the moments $\mathbb{E}^{[\mathbf{F}]}_{(0,0)}[f_1](t)$ and $\mathbb{E}^{[\mathbf{F}]}_{(0,0)}[f_2](t)$ (see Eq. (3)), and of the following quantity:

$$\mathbb{E}^{[\mathbf{F}]}_{(0,1)}[f_i](t) = \int_{D_w} w\, f_i(t,w)\,\mathrm{d}w, \quad i \in \{1,2\}, \tag{4}$$

which represents the average value of energy provided by the energy source NR ($\mathbb{E}^{[\mathbf{F}]}_{(0,1)}[f_1](t)$) and by the energy source R ($\mathbb{E}^{[\mathbf{F}]}_{(0,1)}[f_2](t)$).

The initial condition $\mathbf{f}^0$ is defined as follows:

$$f_i^0(w) = \begin{cases} \dfrac{2}{\sqrt{\pi}} \exp\left(-16\,(w-2.3)^2\right) & \text{if} \quad i = 1, \\ \dfrac{2}{\sqrt{\pi}} \exp\left(-16\,(w-0.7)^2\right) & \text{if} \quad i = 2. \end{cases} \tag{5}$$

Accordingly,

- $\mathbb{E}^{[\mathbf{F}]}_{(0,0)}[f_1^0] = \mathbb{E}^{[\mathbf{F}]}_{(0,0)}[f_2^0] = 0.5$, namely at $t = 0$ the number of customers served by the energy source NR is equal to the number of customers served by the energy source R.
- $\mathbb{E}^{[\mathbf{F}]}_{(0,1)}[f_1^0] > \mathbb{E}^{[\mathbf{F}]}_{(0,1)}[f_2^0]$, namely at $t = 0$ the most part of the energy provided to the customers is produced by the energy source NR.

The numerical simulations aim at investigating the effects of the time-dependent activation parameters on the plan of improvement of the energy quality in order to study the construction of the energy storage. Specifically the optimization process of the network $\mathcal{N}$ relies on the achievement of a virtuous trend which is characterized by two aspects:

1. The most part of the customers should be supplied with the energy produced by the energy source R, i.e. $\mathbb{E}^{[\mathbf{F}]}_{(0,0)}[f_1](t) < \mathbb{E}^{[\mathbf{F}]}_{(0,0)}[f_2](t)$.
2. The most part of the energy provided to the customers should be produced by the energy source R, i.e. $\mathbb{E}^{[\mathbf{F}]}_{(0,1)}[f_1](t) < \mathbb{E}^{[\mathbf{F}]}_{(0,1)}[f_2](t)$.

Remark 1 If $\mathbf{F} = \mathbf{0}$, the mathematical model (1) rewrites as follows:

$$
\begin{aligned}
\partial_t f_1(t,w) = {} & \epsilon_{11}(t)\,(\alpha+\beta)\; f_1(t,w)\int_{D_w} f_1(t,w^*)\,\mathrm{d}w^* \\
& + \epsilon_{12}(t)\,\alpha\; f_1(t,w+\lambda_1)\int_{D_w} f_2(t,w^*)\,\mathrm{d}w^* \\
& + (1-\epsilon_{21}(t))\;\alpha\; f_2(t,w-\lambda_2)\int_{D_w} f_1(t,w^*)\,\mathrm{d}w^* \\
& + (1-\epsilon_{22}(t))\,(\alpha+\beta)\; f_2(t,w)\int_{D_w} f_2(t,w^*)\,\mathrm{d}w^* \\
& - f_1(t,w)\int_{D_w}\left((\alpha+\beta)\; f_1(t,w^*)+\alpha f_2(t,w^*)\right)\mathrm{d}w^*, \\
\partial_t f_2(t,w) = {} & (1-\epsilon_{11}(t))\,(\alpha+\beta)\; f_1(t,w)\int_{D_w} f_1(t,w^*)\,\mathrm{d}w^* \\
& + (1-\epsilon_{12}(t))\;\alpha\; f_1(t,w+\lambda_1)\int_{D_w} f_2(t,w^*)\,\mathrm{d}w^* \\
& + \epsilon_{21}(t)\,\alpha\; f_2(t,w-\lambda_2)\int_{D_w} f_1(t,w^*)\,\mathrm{d}w^* \\
& + \epsilon_{22}(t)\,(\alpha+\beta)\; f_2(t,w)\int_{D_w} f_2(t,w^*)\,\mathrm{d}w^* \\
& - f_2(t,w)\int_{D_w}\left(\alpha\; f_1(t,w^*)+(\alpha+\beta)\; f_2(t,w^*)\right)\mathrm{d}w^*.
\end{aligned}
\tag{6}
$$

The energy allocated into the energy storage is modeled by the following quantity:

$$
\mathbf{E}[\mathbf{F},\mathbf{f}](t) = \mathbb{E}_{(0,1)}[\mathbf{f}](t) - \mathbb{E}^{[\mathbf{F}]}_{(0,1)}[\mathbf{f}](t), \tag{7}
$$

which denotes the difference between the energy $\mathbb{E}^{[\mathbf{F}=\mathbf{0}]}_{(0,1)}[\mathbf{f}](t) = \mathbb{E}_{(0,1)}[\mathbf{f}](t)$ provided to the customers with $\mathbf{F} = \mathbf{0}$ and with $\mathbf{F} \neq \mathbf{0}$, namely $\mathbb{E}^{[\mathbf{F}]}_{(0,1)}[\mathbf{f}](t)$. The network $\mathcal{N}$ determines the amount of energy that has to be allocated into the energy storage. It is worth stressing that $\mathbf{E}[\mathbf{F},\mathbf{f}](t)$ is computed by means of the global (0, 1)-th order moment.

Since the boosted activation of an energy source corresponds to the feeble activation of the other energy source, it is expected that the global macroscopic quantities are not affected by the time-dependent activation of the energy sources. Therefore, the energy allocated into the energy storage should not be affected by the time-dependent phenomena which are mimicked by the time-dependent activation parameters.

The next sections are devoted to the modeling of specific energy sources in order to properly capture their time-dependent properties. The modeling interest is addressed to the

analysis of the reliability of the network $\mathcal{N}$ when the time-dependent efficiency of the energy sources is taken into account.

3 The solar energy source

In this section the renewable energy source R of the network $\mathcal{N}$ is assumed to be a solar energy source S. The activation of the solar energy source can depend on the day–night cycle: it is reduced during the night and reaches its maximum during the day. It is assumed that the solar energy source has an integrated storage which ensures the energy production during the night [36].

Let $g(t) : [0, +\infty[\to [0, 1]$ be the function which mimics the activation of the energy source S. The function $g(t)$ is modeled according to the variation of the solar irradiation over the time proposed in the papers [37,38]. Specifically the function $g(t)$ reaches its maximum during the day and goes towards to zero during the night. The function $g(t)$ is assumed to be a periodic bump function of period $\tau = 2\Delta t + \Delta t_N$, where $2\Delta t \in \mathbb{R}^+$ denotes the duration of the day time interval and $\Delta t_N \in \mathbb{R}^+$ denotes the duration of the night-time interval. For $t \in [0, \tau]$, the function $g(t)$ writes as follows:

$$g(t) = \begin{cases} \exp\left(1 - \dfrac{1}{1 - \left(\frac{t - t_M}{\Delta t}\right)^2}\right) & \text{if} \quad t \in [0, 2\Delta t], \\ 0 & \text{if} \quad t \in]2\Delta t, \tau], \end{cases} \tag{8}$$

where $t_M \in \mathbb{R}^+$ denotes the instant of time characterized by the maximum irradiation. For $t > \tau$, the function $g(t)$ is reproduced periodically (see the Fig. 1). The night-time interval Δt_N can change according to the season and to the geographical position. In particular during the night-time interval the function $g(t) = 0$ (the energy source S is completely inhibited).

The parameters $(\epsilon_{11}(t), \epsilon_{12}(t), \epsilon_{21}(t), \epsilon_{22}(t))$ of the mathematical model (1) are set as follows:

$$\begin{cases} \epsilon_{22}(t) := g(t)\,\epsilon_{22}, \\ \epsilon_{21}(t) := g(t)\,\epsilon_{21}, \\ \epsilon_{11}(t) := (1 - g(t))\,\epsilon_{11}, \\ \epsilon_{12}(t) := (1 - g(t))\,\epsilon_{12}, \end{cases} \tag{9}$$

where $\epsilon_{lj} \in [0, 1]$, for $l, j \in \{1, 2\}$, is a fixed parameter. The activation of the energy source S is promoted during the day ($\epsilon_{22}(t)$ and $\epsilon_{21}(t)$), while the activation of the energy source NR is promoted during the night ($\epsilon_{11}(t)$ and $\epsilon_{12}(t)$).

Bearing all above in mind, the mathematical model (6) now writes:

$$\begin{aligned} \partial_t f_1(t, w) = {} & (1 - g(t))\,\epsilon_{11}\,(\alpha + \beta)\; f_1(t, w) \int_{D_w} f_1(t, w^*)\,\mathrm{d}w^* \\ & + (1 - g(t))\,\epsilon_{12}\,\alpha\; f_1(t, w + \lambda_1) \int_{D_w} f_2(t, w^*)\,\mathrm{d}w^* \\ & + (1 - g(t)\,\epsilon_{21})\;\alpha\; f_2(t, w - \lambda_2) \int_{D_w} f_1(t, w^*)\,\mathrm{d}w^* \\ & + (1 - g(t)\,\epsilon_{22})\,(\alpha + \beta)\;\; f_2(t, w) \int_{D_w} f_2(t, w^*)\,\mathrm{d}w^* \end{aligned}$$

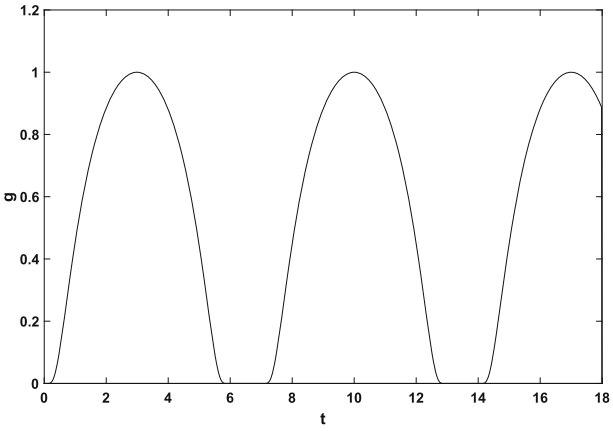

Fig. 1 The function $g(t)$ defined in the Eq. (8) for $\bar{t} = 3$, $\Delta t = 3$ and $\Delta t_N = 1$

$$
\begin{aligned}
&- f_1(t,w) \int_{D_w} \left((\alpha+\beta)\ f_1(t,w^*) + \alpha f_2(t,w^*)\right) \mathrm{d}w^*, \\
\partial_t f_2(t,w) = {} & (1-(1-g(t))\,\epsilon_{11})\,(\alpha+\beta)\ f_1(t,w) \int_{D_w} f_1(t,w^*)\,\mathrm{d}w^* \\
&+ (1-(1-g(t))\,\epsilon_{12})\ \alpha\ f_1(t,w+\lambda_1) \int_{D_w} f_2(t,w^*)\,\mathrm{d}w^* \\
&+ g(t)\,\epsilon_{21}\,\alpha\ f_2(t,w-\lambda_2) \int_{D_w} f_1(t,w^*)\,\mathrm{d}w^* \\
&+ g(t)\,\epsilon_{22}\,(\alpha+\beta)\ f_2(t,w) \int_{D_w} f_2(t,w^*)\,\mathrm{d}w^* \\
&- f_2(t,w) \int_{D_w} \left(\alpha\ f_1(t,w^*) + (\alpha+\beta)\ f_2(t,w^*)\right) \mathrm{d}w^*. \qquad (10)
\end{aligned}
$$

The introduction of time-dependent activation parameters allows to optimize the supply of high-quality energy by the network $\mathcal{N}$. The results are shown by means of the moments $\mathbb{E}_{(0,0)}[f_1](t)$ and $\mathbb{E}_{(0,0)}[f_2](t)$.

The parameters of the model are set as follows: $\alpha = 0.6$, $\beta = 0.1$, $\epsilon_{11} = 0.5 = \epsilon_{22}$, $\epsilon_{12} = 0.3$, $\epsilon_{21} = 0.8$, $\lambda_1 = 0.5$ and $\lambda_2 = 0.6$. If $\epsilon_{12} < \epsilon_{21}$ a virtuous trend is promoted; the magnitudes of λ_1 and λ_2 allow to capture the heterogeneity of the energy production. The interested reader is referred to [34] for more details concerning a sensitivity analysis on the parameters. The parameters of the function $g(t)$ in the Eq. (8) are set as follows: $t_M = 3$ and $\Delta t = 3$. The numerical simulations investigate the effect of the duration of Δt_N on the energy production.

It is expected that the increase in the duration of the night-time interval Δt_N reduces the number $\mathbb{E}_{(0,0)}[f_2](t)$ of customers served by the energy produced by the energy source S.

For null and low values of Δt_N, the trend is still virtuous and $\mathbb{E}_{(0,0)}[f_1](t) < \mathbb{E}_{(0,0)}[f_2](t)$ for all t (see the Fig. 2). When Δt_N increases an alternate trend appears, which is virtuous during the day, i.e. when $g(t) > 0$, and non virtuous during the night, i.e. when $g(t) = 0$. As shown in Fig. 3, the duration of the time interval characterized by a virtuous trend, namely $\mathbb{E}_{(0,0)}[f_1](t) < \mathbb{E}_{(0,0)}[f_2](t)$, decreases with the increase in Δt_N.

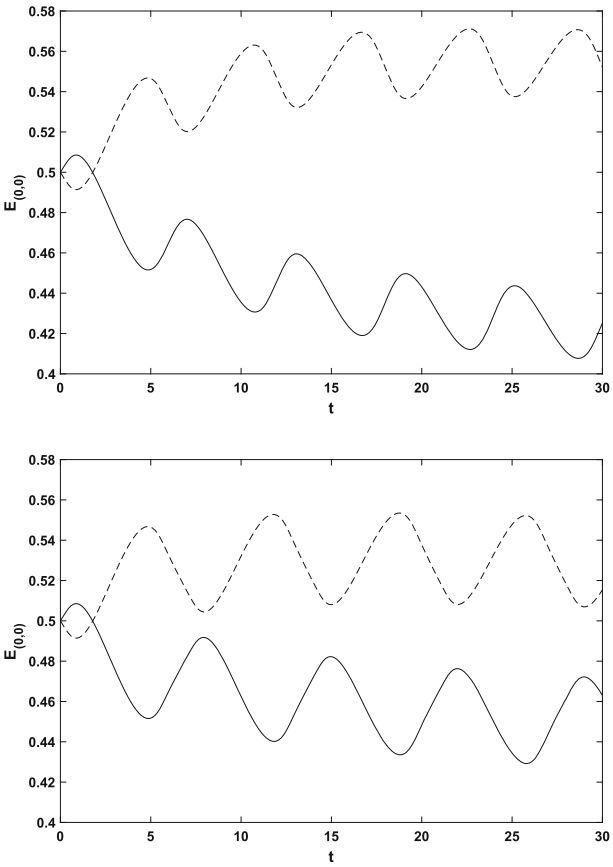

Fig. 2 The time evolution of the moments $\mathbb{E}_{(0,0)}[f_1](t)$ related to the energy source NR (solid line) and $\mathbb{E}_{(0,0)}[f_2](t)$ related to the energy source S (dashed line), for $\Delta t_N = 0$ (first row panel) and $\Delta t_N = 1$ (second row panel)

The introduction of time-dependent activation parameters affects also the average energy that each energy source yields to the customers, namely the moments $\mathbb{E}_{(0,1)}[f_1](t)$ and $\mathbb{E}_{(0,1)}[f_2](t)$.

As shown in the Figs. 4 and 5, the increase in magnitude of Δt_N reduces the average energy $\mathbb{E}_{(0,1)}[f_2](t)$ produced by the energy source S. Indeed the virtuous trend, i.e. $\mathbb{E}_{(0,1)}[f_2](t) > \mathbb{E}_{(0,1)}[f_1](t)$ for all t, is delayed (see the second row panel of the Fig. 4) and it follows the day–night alternance until $t \simeq 35$; for $t > 35$ the trend is completely virtuous because $\mathbb{E}_{(0,1)}[f_2](t) > \mathbb{E}_{(0,1)}[f_1](t)$ for all t even if the periodic time fluctuations persist. As shown in Fig. 5, the scenario changes when the length of the night-time interval Δt_N increases. The trend follows the day–night alternance but the production of energy by the energy source S decreases.

An important investigation is related to the evolution of the first inversion time t^* defined as follows:

$$t^* = \min_{t \in]0,+\infty[} \{t : \mathbb{E}_{(0,1)}[f_1](t) = \mathbb{E}_{(0,1)}[f_2](t)\}. \tag{11}$$

Figure 6 shows how t^* evolves with respect to the duration of the night-time interval Δt_N (see the Table 1 for the data). As shown in Fig. 6, the increase in the length of Δt_N implies the

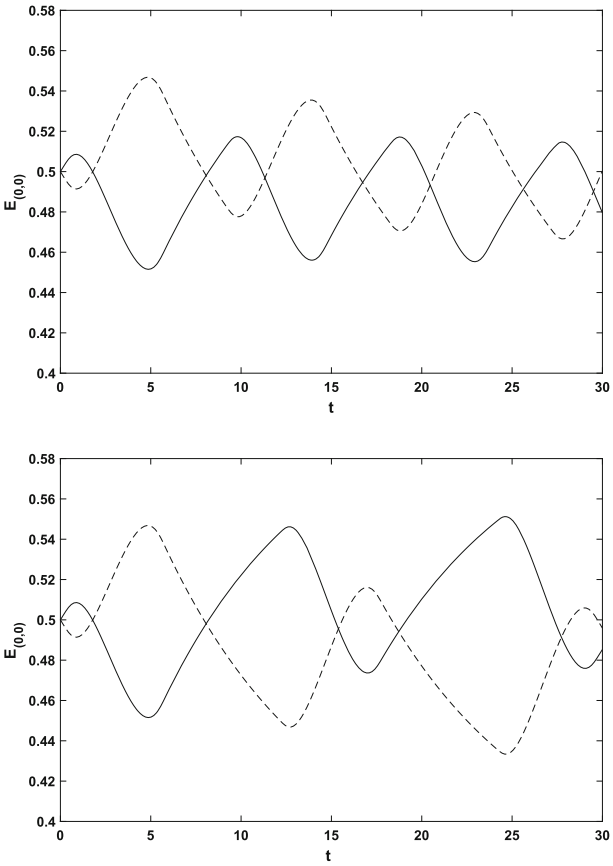

Fig. 3 The time evolution of the moments $\mathbb{E}_{(0,0)}[f_1](t)$ related to the energy source NR (solid line) and $\mathbb{E}_{(0,0)}[f_2](t)$ related to the energy source S (dashed line), for $\Delta t_N = 3$ (first row panel) and $\Delta t_N = 6$ (second row panel)

increase in t^*, namely the inversion of the initial scenario is delayed as it is expected since the duration of Δt_N affects the activation of the energy source S. Moreover, the evolution of t^* can exhibit discontinuities which depend on the difference $\epsilon_{21} - \epsilon_{12} > 0$, namely as the virtuous trend becomes weaker.

The construction of the energy storage is taken into account by the mathematical model (1) which rewrites as follows:

$$
\begin{aligned}
&\partial_t f_1(t,w) + F\,\partial_w\left(\left(1-\alpha_{(2,2)}[\mathbf{f}](t)\,w\right) f_1(t,w)\right)\\
&= (1-g(t))\,\epsilon_{11}\,(\alpha+\beta)\; f_1(t,w)\int_{D_w} f_1(t,w^*)\,\mathrm{d}w^*\\
&\quad + (1-g(t))\,\epsilon_{12}\,\alpha\, f_1(t,w+\lambda_1)\int_{D_w} f_2(t,w^*)\,\mathrm{d}w^*\\
&\quad + (1-g(t)\,\epsilon_{21})\;\alpha\, f_2(t,w-\lambda_2)\int_{D_w} f_1(t,w^*)\,\mathrm{d}w^*\\
&\quad + (1-g(t)\,\epsilon_{22})\,(\alpha+\beta)\; f_2(t,w)\int_{D_w} f_2(t,w^*)\,\mathrm{d}w^*
\end{aligned}
$$

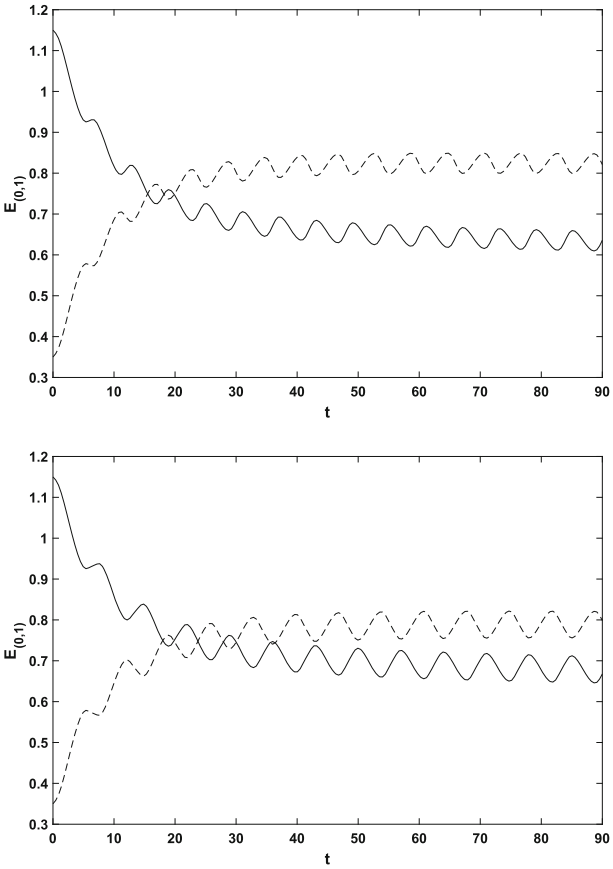

Fig. 4 The time evolution of the moments $\mathbb{E}_{(0,1)}[f_1](t)$ related to the energy source NR (solid line) and $\mathbb{E}_{(0,1)}[f_2](t)$ related to the energy source S (dashed line), for $\Delta t_N = 0$ (first row panel) and $\Delta t_N = 1$ (second row panel)

$$
\begin{aligned}
&- f_1(t,w)\int_{D_w}\left((\alpha+\beta)\ f_1(t,w^*)+\alpha f_2(t,w^*)\right)\mathrm{d}w^*,\\
&\partial_t f_2(t,w)+F\,\partial_w\left(\left(1-\alpha_{(2,2)}[\mathbf{f}](t)\,w\right)f_2(t,w)\right)\\
&=(1-(1-g(t))\,\epsilon_{11})\,(\alpha+\beta)\ f_1(t,w)\int_{D_w} f_1(t,w^*)\,\mathrm{d}w^*\\
&\quad+(1-(1-g(t))\,\epsilon_{12})\ \alpha\ f_1(t,w+\lambda_1)\int_{D_w} f_2(t,w^*)\,\mathrm{d}w^*\\
&\quad+g(t)\,\epsilon_{21}\,\alpha\ f_2(t,w-\lambda_2)\int_{D_w} f_1(t,w^*)\,\mathrm{d}w^*\\
&\quad+g(t)\,\epsilon_{22}\,(\alpha+\beta)\ f_2(t,w)\int_{D_w} f_2(t,w^*)\,\mathrm{d}w^*\\
&\quad- f_2(t,w)\int_{D_w}\left(\alpha\ f_1(t,w^*)+(\alpha+\beta)\ f_2(t,w^*)\right)\mathrm{d}w^*\\
&\quad- f_1(t,w)\int_{D_w}\left((\alpha+\beta)\ f_1(t,w^*)+\alpha f_2(t,w^*)\right)\mathrm{d}w^*,
\end{aligned}
\tag{12}
$$

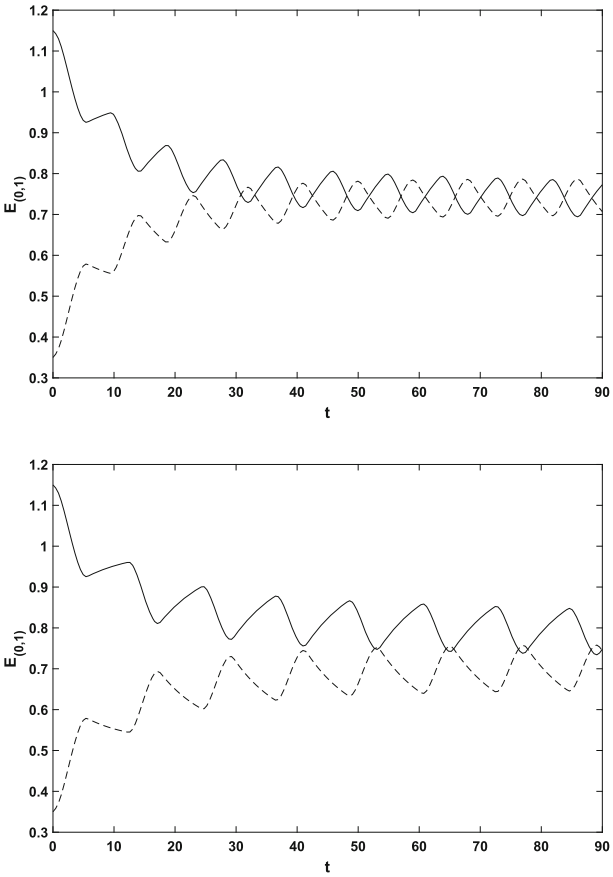

Fig. 5 The time evolution of the moments $\mathbb{E}_{(0,1)}[f_1](t)$ related to the energy source NR (solid line) and $\mathbb{E}_{(0,1)}[f_2](t)$ related to the energy source S (dashed line), for $\Delta t_N = 3$ (first row panel) and $\Delta t_N = 6$ (second row panel)

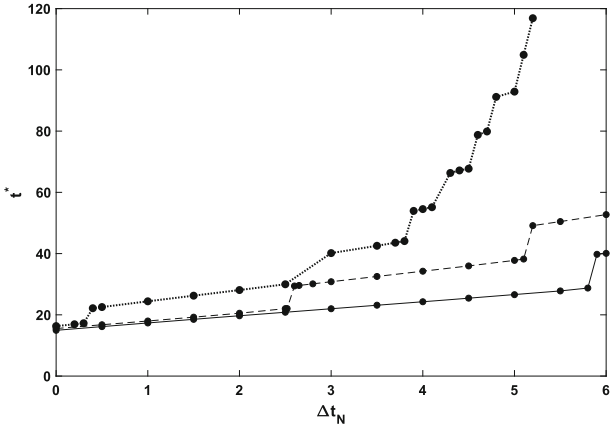

Fig. 6 The first inversion time t^* versus Δt_N, for $(\epsilon_{12}, \epsilon_{21}) = (0.2, 0.9)$ (solid line), for $(\epsilon_{12}, \epsilon_{21}) = (0.3, 0.8)$ (dashed line), for $(\epsilon_{12}, \epsilon_{21}) = (0.4, 0.7)$ (dot line)

Table 1 The first inversion time t^* versus Δt_N for different magnitudes of ϵ_{12} and ϵ_{21}

$(\epsilon_{12}, \epsilon_{21}) = (0.2, 0.9)$		$(\epsilon_{12}, \epsilon_{21}) = (0.3, 0.8)$		$(\epsilon_{12}, \epsilon_{21}) = (0.4, 0.7)$	
Δt_N	t^*	Δt_N	t^*	Δt_N	t^*
0	14.95	0	15.52	0	16.32
0.5	16.15	0.5	16.76	0.2	16.92
1	17.35	1	17.98	0.3	17.25
1.5	18.52	1.5	19.236	0.4	22.16
2	19.69	2	20.52	0.5	22.54
2.5	20.85	2.5	22.02	1	24.41
3	21.99	2.52	22.04	1.5	26.26
3.5	23.14	2.6	29.42	2	28.09
4	24.27	2.65	29.6	2.5	29.98
4.5	25.45	2.8	30.11	3	40.16
5	26.59	3	30.81	3.5	42.55
5.5	27.81	3.5	32.53	3.7	43.55
5.8	28.74	4	34.25	3.8	44.08
5.9	39.77	4.5	35.97	3.9	53.94
6	40.08	5	37.78	4	54.53
–	–	5.1	38.21	4.1	55.15
–	–	5.2	49.13	4.3	66.33
–	–	5.5	50.46	4.4	67.16
–	–	6	52.73	4.5	67.73
–	–	–	–	4.6	78.76
–	–	–	–	4.7	79.88
–	–	–	–	4.8	91.17
–	–	–	–	5	92.89
–	–	–	–	5.1	104.9
–	–	–	–	5.2	116.87
–	–	–	–	5.5	> 250

where the thermostat term $\alpha_{(2,2)}[\mathbf{f}](t)$ can be recovered by the Eq. (2).

Figure 7 shows the time evolution of the energy $\mathbf{E}[\mathbf{F}, \mathbf{f}](t)$ allocated into the energy storage for different magnitudes F of the external force and for different lengths of the night-time interval Δt_N. The different panels of the Fig. 7 show that the construction of the energy storage is not influenced by the periodic fluctuations of the function $g(t)$. This result underlines how the construction of the energy storage is stable with respect to the time-dependent activation of the energy source. This feature is extremely important from the point of view of the reliability of the network $\mathcal{N}$. Moreover, Fig. 7 shows that the energy $\mathbf{E}[\mathbf{F}, \mathbf{f}](t)$ allocated into the energy storage increases over time and reaches an asymptotic value which depends on the magnitude F. The asymptotic value can be considered as the maximum amount of energy allocated into the energy storage for a certain magnitude F of the external force. As F increases, the amount of energy allocated into the storage increases. The different panels of the Fig. 7 show a slight difference: as Δt_N increases, the allocation of energy into storage is

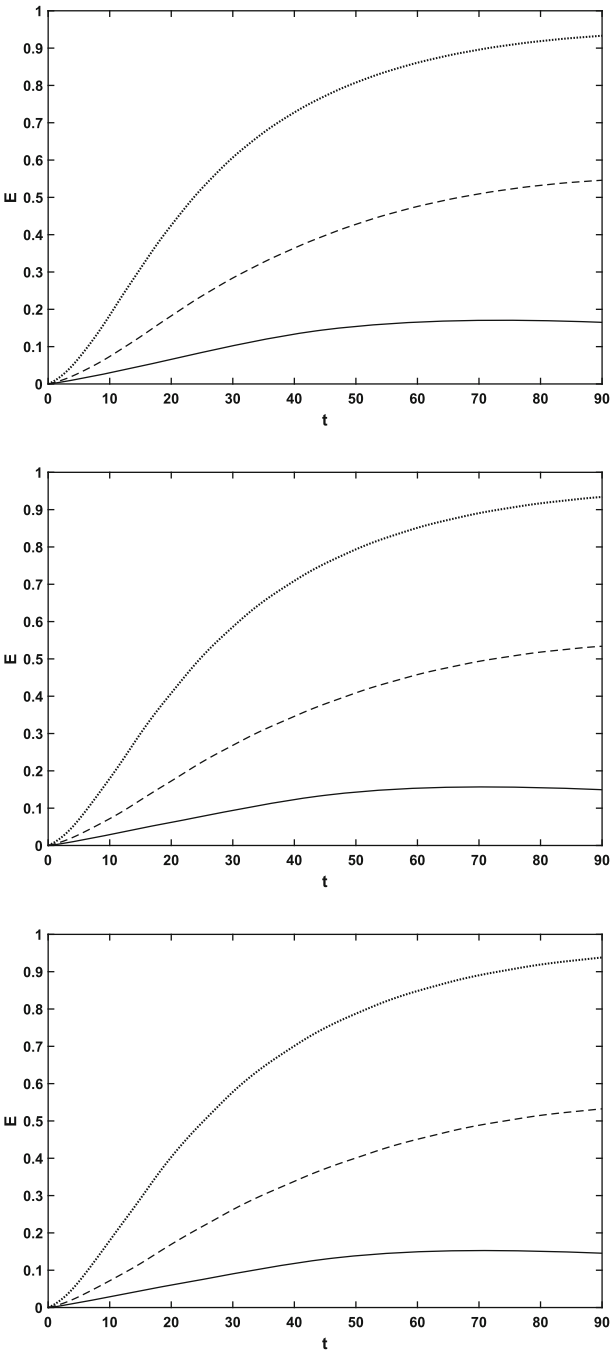

Fig. 7 The time evolution of the energy $\mathbf{E}[\mathbf{F}, \mathbf{f}](t)$ allocated into the energy storage for $\Delta t_N = 0$ (first row panel), for $\Delta t_N = 3$ (second row panel) and for $\Delta t_N = 6$ (third row panel), for $F = 0.05$ (solid line), for $F = 0.1$ (dashed line) and for $F = 0.2$ (dot line)

delayed. This means that as the trend becomes less virtuous, the energy $\mathbf{E}[\mathbf{F}, \mathbf{f}](t)$ increases more slowly.

This interpretation is confirmed by the Fig. 8 which shows the time evolution of the global $(0, 1)$-order moment $\mathbb{E}^{[\mathbf{F}]}_{(0,1)}[\mathbf{f}](t)$ for different magnitudes F of the external force and for different values of the night time interval Δt_N. The increase in the magnitude F reduces the amount of energy $\mathbb{E}^{[\mathbf{F}]}_{(0,1)}[\mathbf{f}](t)$ directly provided to the customers.

It is worth stressing that, if the numerical simulations are carried out beyond the asymptotic values, the numerical model stops describing the construction of the energy storage: the energy $\mathbf{E}[\mathbf{F}, \mathbf{f}](t)$ starts decreasing while the energy $\mathbb{E}^{[\mathbf{F}]}_{(0,1)}[\mathbf{f}](t)$ increases.

4 The wind energy source

In this section the renewable energy source R is assumed to be a wind energy source W. As known, the energy produced by a wind turbine depends on the speed of the wind. In particular, the power curve of a wind turbine depends on technical and engineering aspects and typically exhibits the following characteristics (see [39] for more details):

- The energy production is negligible under a certain cut-in speed v_{in} of the wind.
- The energy production increases with the wind speed until a certain rated speed v_r that characterizes the maximum value of the energy produced by the turbine.
- The energy production does not change with the wind speed and remains constant until a certain cut-out speed v_{out}, which is the maximum speed value at which the turbine produces energy.
- If the speed of the wind is bigger than the cut-out speed v_{out} the turbine is braked in order to avoid damages to the rotor.

The power curve depicted in Fig. 9 (see [40]) is assumed to have the cut-in speed for $v_{\text{in}} = 5$ m/s, the rated speed for $v_r = 15$ m/s, the cut-out speed for $v_{\text{out}} = 25$ m/s, while the rate of energy production E, for a wind speed $v_{\text{in}} \le v \le v_r$, is set as $E = K\, v^3$, where $K \in \mathbb{R}^+$ is a constant depending on the density of the air and on the design of the turbine, see [41,42]. The wind speed v is distributed according to the following two-parameter Weibull function [43]:

$$f(v) = \frac{a}{c}\left(\frac{v}{c}\right)^{a-1} e^{-\left(\frac{v}{c}\right)^a}, \quad v \in \mathbb{R}^+ \tag{13}$$

where $a, c \in \mathbb{R}^+$ are the shape parameter and the scale parameter, respectively.

A stochastic term $\Lambda(t) : [0, +\infty[\to [0, 1]$ is introduced in the mathematical model (1) in order to model the effects of the wind speed on the efficiency of the energy source W. In particular, the Weibull distribution is employed to generate random values $v(t)$ of the wind speed for each instant of time t. The speed value is compared to the power curve shown in Fig. 9 in order to determine the value of $\Lambda(t)$. Accordingly, at each instant of time t, the stochastic term $\Lambda(t)$ writes as follows:

$$\Lambda(t) = \begin{cases} 0 & \text{if } \ v(t) < v_{\text{in}} = 5\,\text{m/s}, \\ 0.5\left(1 + \left(\dfrac{v(t)}{v_r}\right)^3\right) & \text{if } \ v_{\text{in}} \le v(t) \le v_r = 15\,\text{m/s}, \\ 1 & \text{if } \ v_r < v(t) \le v_{\text{out}} = 25\,\text{m/s}, \\ 0 & \text{if } \ v(t) > v_{\text{out}}. \end{cases} \tag{14}$$

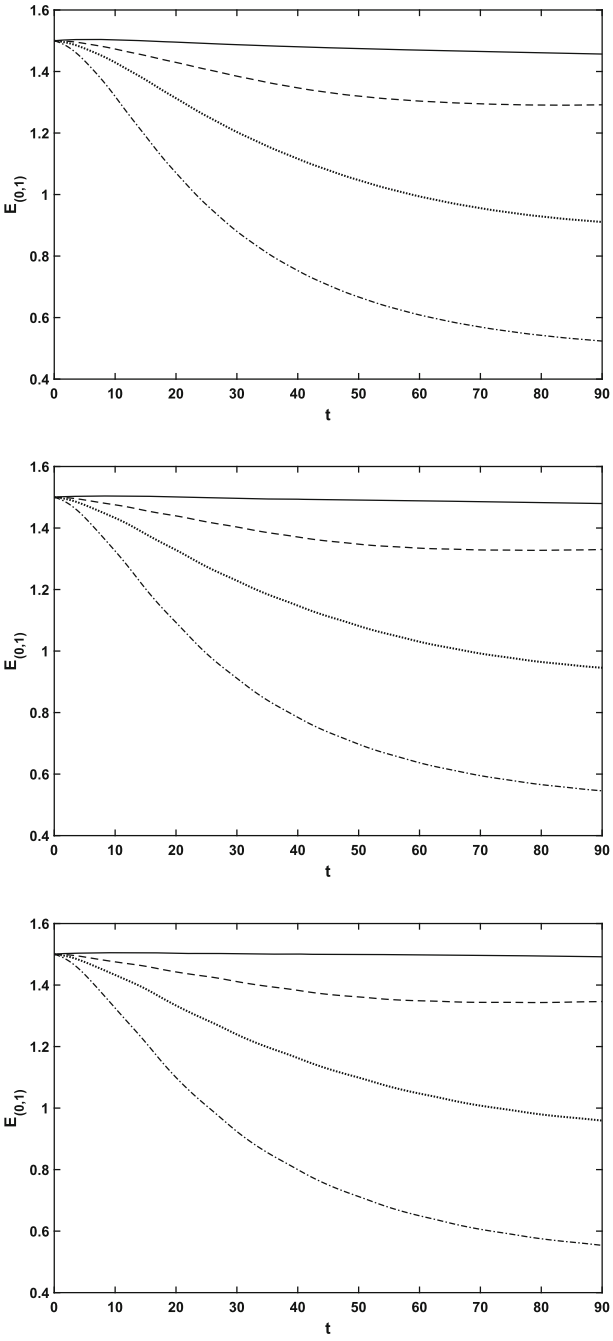

Fig. 8 The time evolution of the global moment $\mathbb{E}^{[\mathbf{F}]}_{(0,1)}[\mathbf{f}](t)$, for $\Delta t_N = 0$ (first row panel), for $\Delta t_N = 3$ (second row panel) and for $\Delta t_N = 6$ (third panel), for $F = 0$ (solid line), for $F = 0.05$ (dashed line), for $F = 0.1$ (dot line) and for $F = 0.2$ (dashed-dot line)

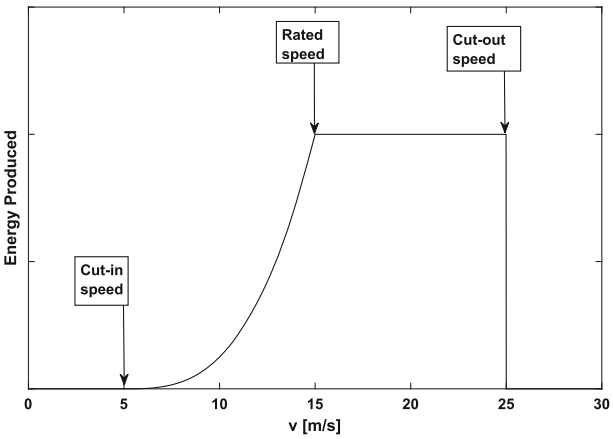

Fig. 9 The power curve of a wind turbine for $v_{\text{in}} = 5$, $v_r = 15$ and $v_{\text{out}} = 25$

The parameters $(\epsilon_{11}(t), \epsilon_{12}(t), \epsilon_{21}(t), \epsilon_{22}(t))$ of the mathematical model (1) are set as follows:

$$\begin{cases} \epsilon_{22}(t) := \Lambda(t)\,\epsilon_{22}, \\ \epsilon_{21}(t) := \Lambda(t)\,\epsilon_{21}, \\ \epsilon_{11}(t) := (1-\Lambda(t))\,\epsilon_{11}, \\ \epsilon_{12}(t) := (1-\Lambda(t))\,\epsilon_{12}, \end{cases} \tag{15}$$

where $\epsilon_{lj} \in [0, 1]$, for $l, j \in \{1, 2\}$, is a fixed parameter. The activation of the energy source W is promoted when the speed of the wind is high ($\epsilon_{22}(t)$ and $\epsilon_{21}(t)$), while the activation of the energy source NR is promoted when the speed of the wind is low or higher than v_{out} ($\epsilon_{11}(t)$ and $\epsilon_{12}(t)$).

Bearing all above in mind, the mathematical model (6) now writes:

$$\begin{aligned} \partial_t f_1(t,w) = {} & (1-\Lambda(t))\,\epsilon_{11}\,(\alpha+\beta)\; f_1(t,w) \int_{D_w} f_1(t,w^*)\,\mathrm{d}w^* \\ & + (1-\Lambda(t))\,\epsilon_{12}\,\alpha\; f_1(t,w+\lambda_1) \int_{D_w} f_2(t,w^*)\,\mathrm{d}w^* \\ & + (1-\Lambda(t)\,\epsilon_{21})\;\alpha\; f_2(t,w-\lambda_2) \int_{D_w} f_1(t,w^*)\,\mathrm{d}w^* \\ & + (1-\Lambda(t)\,\epsilon_{22})\,(\alpha+\beta)\; f_2(t,w) \int_{D_w} f_2(t,w^*)\,\mathrm{d}w^* \\ & - f_1(t,w) \int_{D_w} \big((\alpha+\beta)\; f_1(t,w^*) + \alpha f_2(t,w^*)\big)\,\mathrm{d}w^*, \\ \partial_t f_2(t,w) = {} & (1-(1-\Lambda(t))\,\epsilon_{11})\,(\alpha+\beta)\; f_1(t,w) \int_{D_w} f_1(t,w^*)\,\mathrm{d}w^* \\ & + (1-(1-\Lambda(t))\,\epsilon_{12})\;\alpha\; f_1(t,w+\lambda_1) \int_{D_w} f_2(t,w^*)\,\mathrm{d}w^* \\ & + \Lambda(t)\,\epsilon_{21}\,\alpha\; f_2(t,w-\lambda_2) \int_{D_w} f_1(t,w^*)\,\mathrm{d}w^* \end{aligned}$$

$$+ \Lambda(t)\,\epsilon_{22}\,(\alpha+\beta)\;f_2(t,w)\int_{D_w} f_2(t,w^*)\,\mathrm{d}w^*$$
$$- f_2(t,w)\int_{D_w}\left(\alpha\, f_1(t,w^*)+(\alpha+\beta)\;f_2(t,w^*)\right)\mathrm{d}w^*. \tag{16}$$

The parameters are set as follows: $\alpha = 0.6$, $\beta = 0.1$, $\epsilon_{11} = 0.5 = \epsilon_{22}$, $\epsilon_{12} = 0.3$, $\epsilon_{21} = 0.8$, $\lambda_1 = 0.5$ and $\lambda_2 = 0.6$.

The fluctuations of the wind speed affect the energy production of the energy source W. The modeling interest is addressed to analyze the effect on the plan of improvement of the quality of the energy provided to the customers by depicting the number of customers served by the two energy sources, $\mathbb{E}_{(0,0)}[f_1](t)$ and $\mathbb{E}_{(0,0)}[f_2](t)$, and the average energy supplied to the customers, $\mathbb{E}_{(0,1)}[f_1](t)$ and $\mathbb{E}_{(0,1)}[f_2](t)$.

The first proposed scenario relies on the values $a = 3$ and $c = 4\,$m/s for the city of Cergy-Pontoise in France in the period $10/04/2019 - 25/04/2019$ [44]. The corresponding Weibull distribution is shown in the first row panel of the Fig. 10. As the second and third row panels of Fig. 10 show, the trend is not virtuous. A large number of the customers are supplied by the energy source NR, i.e. $\mathbb{E}_{(0,0)}[f_1](t) > \mathbb{E}_{(0,0)}[f_2](t)$ for all t, and the most part of the energy is produced by the energy source NR, i.e. $\mathbb{E}_{(0,1)}[f_1](t) > \mathbb{E}_{(0,1)}[f_2](t)$ for all t. The increase in the magnitude of c models the increase in the average wind speed. The first row panel of the Fig. 11 shows the Weibull distribution for $a = 3$ and $c = 10\,$m/s. As it is shown in the second and third row panels of Fig. 11, in this scenario the bigger speed of the wind allows to promote the virtuous trend, namely $\mathbb{E}_{(0,0)}[f_1](t) < \mathbb{E}_{(0,0)}[f_2](t)$ for all t and $\mathbb{E}_{(0,1)}[f_1](t) < \mathbb{E}_{(0,1)}[f_2](t)$ for all t. The increase in the magnitude of a reduces the dispersion of the wind speed distribution. In particular, the first row panel of Fig. 12 shows the Weibull distribution for $a = 6$ and $c = 10$ m/s. The second and third row panels of Fig. 12 show that the trend is still virtuous, but the time evolution of the moments exhibits less fluctuations with respect to Fig. 11. On the contrary, the decrease in the magnitude of a produces a bigger dispersion of the wind speed distribution. An example of this scenario is depicted by the Fig. 13 for $a = 2$ and $c = 10$ m/s. The first row panel shows the related Weibull distribution, the second and third row panels show the time evolution of $\mathbb{E}_{(0,0)}[f_i](t)$ and $\mathbb{E}_{(0,1)}[f_i](t)$, respectively, for $i \in \{1,2\}$. The trend is still virtuous but the higher dispersion of the values of the wind speed produces fluctuations in the time evolution of the moments.

The construction of the energy storage is mimicked by the mathematical model (1) which rewrites as follows:

$$\begin{aligned}
&\partial_t f_1(t,w) + F\,\partial_w\left(\left(1-\alpha_{(2,2)}[\mathbf{f}](t)\,w\right)\,f_1(t,w)\right)\\
&= (1-\Lambda(t))\,\epsilon_{11}\,(\alpha+\beta)\;f_1(t,w)\int_{D_w} f_1(t,w^*)\,\mathrm{d}w^*\\
&\quad + (1-\Lambda(t))\,\epsilon_{12}\,\alpha\,f_1(t,w+\lambda_1)\int_{D_w} f_2(t,w^*)\,\mathrm{d}w^*\\
&\quad + (1-\Lambda(t)\,\epsilon_{21})\;\alpha\;f_2(t,w-\lambda_2)\int_{D_w} f_1(t,w^*)\,\mathrm{d}w^*\\
&\quad + (1-\Lambda(t)\,\epsilon_{22})\,(\alpha+\beta)\;f_2(t,w)\int_{D_w} f_2(t,w^*)\,\mathrm{d}w^*\\
&\quad - f_1(t,w)\int_{D_w}\left((\alpha+\beta)\;f_1(t,w^*)+\alpha f_2(t,w^*)\right)\mathrm{d}w^*,\\
&\partial_t f_2(t,w) + F\,\partial_w\left(\left(1-\alpha_{(2,2)}[\mathbf{f}](t)\,w\right)\,f_2(t,w)\right)
\end{aligned}$$

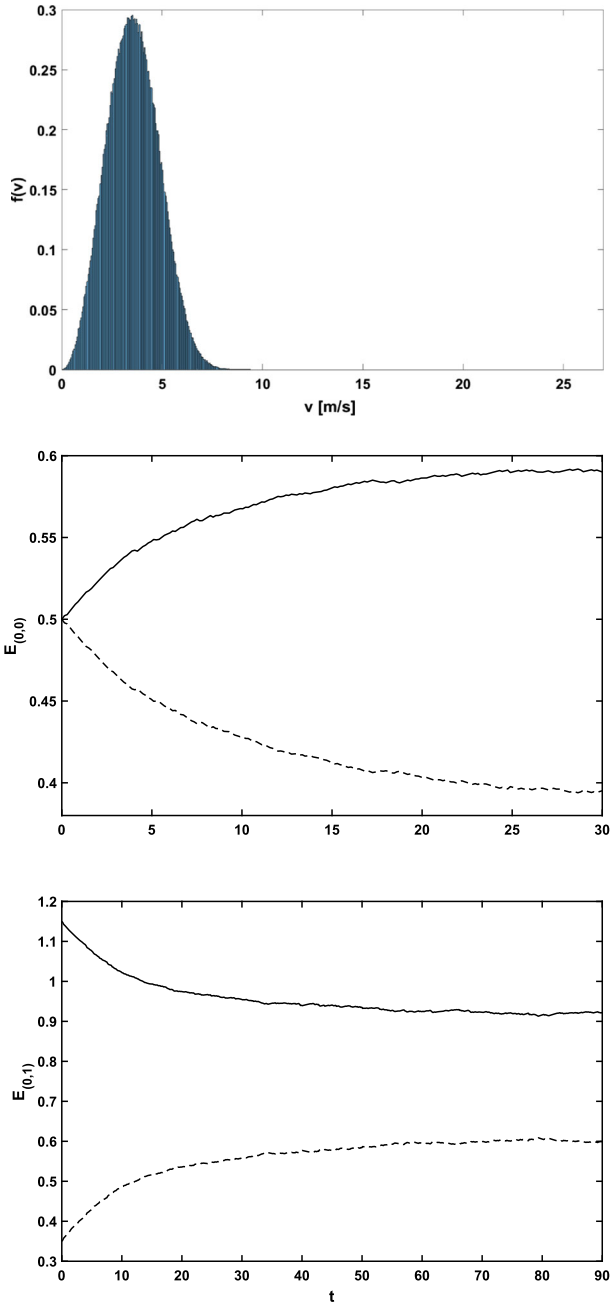

Fig. 10 The Weibull distribution $f(v)$ (first row panel), the time evolution of the moments $\mathbb{E}_{(0,0)}[f_1](t)$ related to the energy source NR (second row panel-solid line) and $\mathbb{E}_{(0,0)}[f_2](t)$ related to the energy source W (second row panel-dashed line), the time evolution of the moments $\mathbb{E}_{(0,1)}[f_1](t)$ related to the energy source NR (third row panel-solid line) and $\mathbb{E}_{(0,1)}[f_2](t)$ related to the energy source W (third row panel-dashed line), for $a = 3$ and $c = 4$ m/s

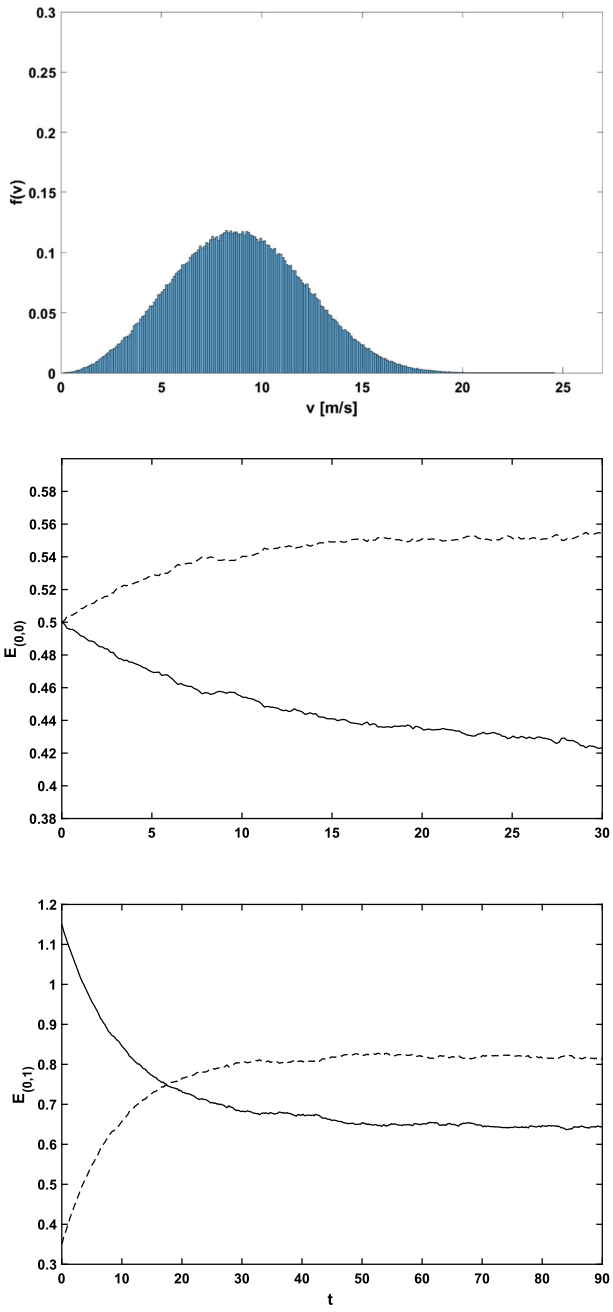

Fig. 11 The Weibull distribution $f(v)$ (first row panel), the time evolution of the moments $\mathbb{E}_{(0,0)}[f_1](t)$ related to the energy source NR (second row panel-solid line) and $\mathbb{E}_{(0,0)}[f_2](t)$ related to the energy source W (second row panel-dashed line), the time evolution of the moments $\mathbb{E}_{(0,1)}[f_1](t)$ related to the energy source NR (third row panel-solid line) and $\mathbb{E}_{(0,1)}[f_2](t)$ related to the energy source W (third row panel-dashed line), for $a = 3$ and $c = 10$ m/s

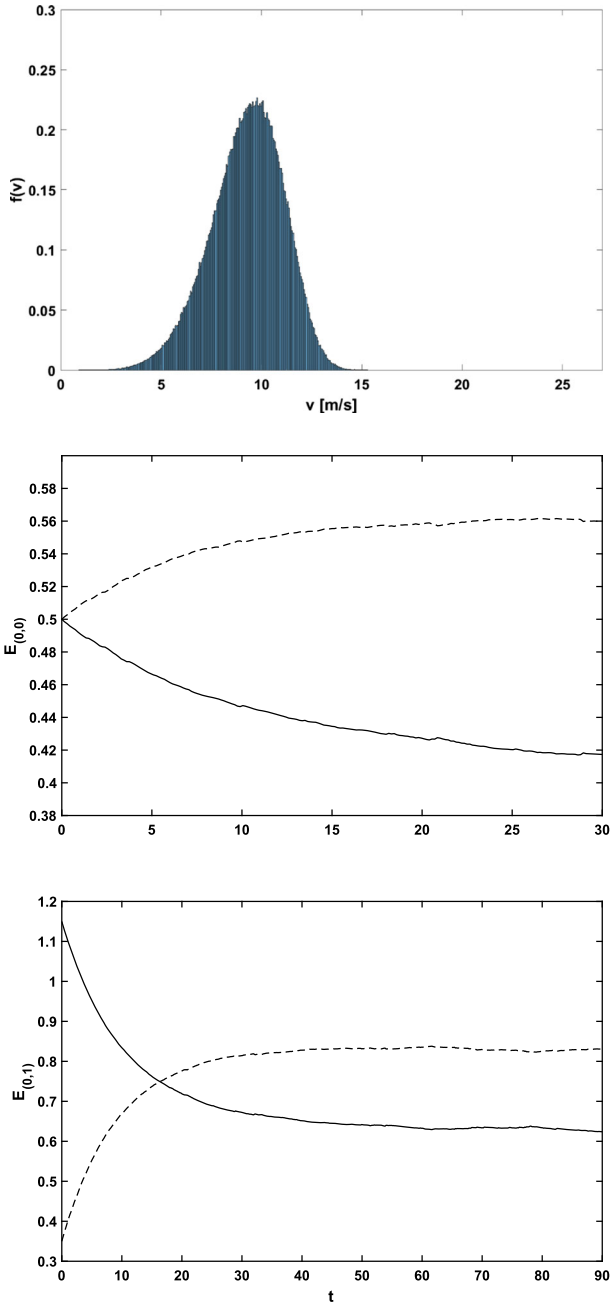

Fig. 12 The Weibull distribution $f(v)$ (first row panel), the time evolution of the moments $\mathbb{E}_{(0,0)}[f_1](t)$ related to the energy source NR (second row panel-solid line) and $\mathbb{E}_{(0,0)}[f_2](t)$ related to the energy source W (second row panel-dashed line), the time evolution of the moments $\mathbb{E}_{(0,1)}[f_1](t)$ related to the energy source NR (third row panel-solid line) and $\mathbb{E}_{(0,1)}[f_2](t)$ related to the energy source W (third row panel-dashed line), for $a = 6$ and $c = 10$ m/s

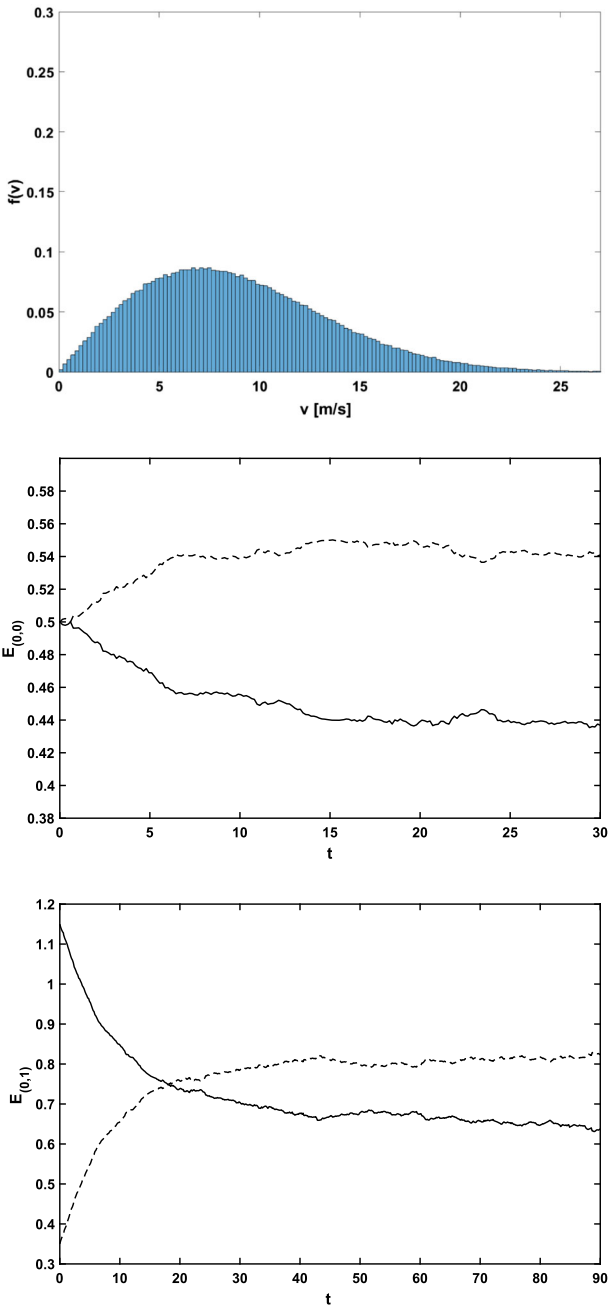

Fig. 13 The Weibull distribution $f(v)$ (first row panel), the time evolution of the moments $\mathbb{E}_{(0,0)}[f_1](t)$ related to the energy source NR (second row panel-solid line) and $\mathbb{E}_{(0,0)}[f_2](t)$ related to the energy source W (second row panel-dashed line), the time evolution of the moments $\mathbb{E}_{(0,1)}[f_1](t)$ related to the energy source NR (third row panel-solid line) and $\mathbb{E}_{(0,1)}[f_2](t)$ related to the energy source W (third row panel-dashed line), for $a = 2$ and $c = 10$ m/s

$$
\begin{aligned}
&= (1-(1-\Lambda(t))\,\epsilon_{11})\,(\alpha+\beta)\;f_1(t,w)\int_{D_w} f_1(t,w^*)\,\mathrm{d}w^* \\
&+ (1-(1-\Lambda(t))\,\epsilon_{12})\;\alpha\;f_1(t,w+\lambda_1)\int_{D_w} f_2(t,w^*)\,\mathrm{d}w^* \\
&+ \Lambda(t)\epsilon_{21}\,\alpha\;f_2(t,w-\lambda_2)\int_{D_w} f_1(t,w^*)\,\mathrm{d}w^* \\
&+ \Lambda(t)\epsilon_{22}\,(\alpha+\beta)\;f_2(t,w)\int_{D_w} f_2(t,w^*)\,\mathrm{d}w^* \\
&- f_2(t,w)\int_{D_w}\left(\alpha\;f_1(t,w^*)+(\alpha+\beta)\;f_2(t,w^*)\right)\mathrm{d}w^* \\
&- f_1(t,w)\int_{D_w}\left((\alpha+\beta)\;f_1(t,w^*)+\alpha f_2(t,w^*)\right)\mathrm{d}w^*, \qquad (17)
\end{aligned}
$$

where the thermostat term $\alpha_{(2,2)}[\mathbf{f}](t)$ can be recovered by the Eq. (2).

The computational analysis is devoted to study the effect of the fluctuations of the speed of the wind on the amount of energy $\mathbf{E}[\mathbf{F},\mathbf{f}](t)$ allocated into the storage. Figure 14 shows that the energy $\mathbf{E}[\mathbf{F},\mathbf{f}](t)$ allocated into the storage is not affected by the different wind scenarios: the fluctuations of the speed of the wind have no influence on the construction process of the energy storage. The energy $\mathbf{E}[\mathbf{F},\mathbf{f}](t)$ allocated to the storage increases over time and reaches an asymptotic value, whose magnitude increases with the increase in the magnitude F. Consequently, the increase in the magnitude F causes the decrease in the average value of energy $\mathbb{E}^{[\mathbf{F}]}_{(0,1)}[\mathbf{f}](t)$ directly provided to the customers (see Fig. 15). The different wind scenarios do not affect the time evolution of the global moment $\mathbb{E}^{[\mathbf{F}]}_{(0,1)}[\mathbf{f}](t)$.

It is worth stressing that the scenario related to $a = 3$ and $c = 4$ m/s is characterized by a delay in the allocation of the energy $\mathbf{E}[\mathbf{F},\mathbf{f}](t)$ into the energy storage, as it can be noticed by the comparison of the panels of the Fig. 14. This phenomenon is caused by the non virtuous trend which characterizes this scenario and, as already stressed in the previous section, slows down the construction of the energy storage.

As stated in the previous section, the computational analysis is performed for a timescale which allows to observe the allocation of the energy into energy storage, namely the increase in $\mathbf{E}[\mathbf{F},\mathbf{f}](t)$ and the related decrease in $\mathbb{E}^{[\mathbf{F}]}_{(0,1)}[\mathbf{f}](t)$.

5 The fossil fuel energy source

This section is devoted to the modeling of the economical aspects which can affect the non-renewable energy source NR. Specifically the activation of the non-renewable energy source can depend on the trend of the fossil fuel price. The fluctuations in the fossil fuel price can be taken into account in the mathematical model (1) by introducing a stochastic term which mimics the random character of the market trend, see [45–47]. Specifically, let $\Gamma(t) : [0,+\infty[\to [0,1]$ be a stochastic process which models the behavior of the fossil fuel price. It is assumed that the fossil fuel price usually assumes a reference price, related to $\Gamma(t) = 0.5$. If the market trend is characterized by the increase in the fossil fuel price, then $\Gamma(t)$ takes with higher probability values which are bigger than 0.5; on the contrary, if the fossil fuel price decreases, then $\Gamma(t)$ takes with higher probability values which are lower than 0.5. It is assumed that, for all $t \in [0,+\infty[$, the values of $\Gamma(t)$ are described by the probability density function $\rho(\Gamma)$. The distribution function $\rho(\Gamma)$ can be modified in

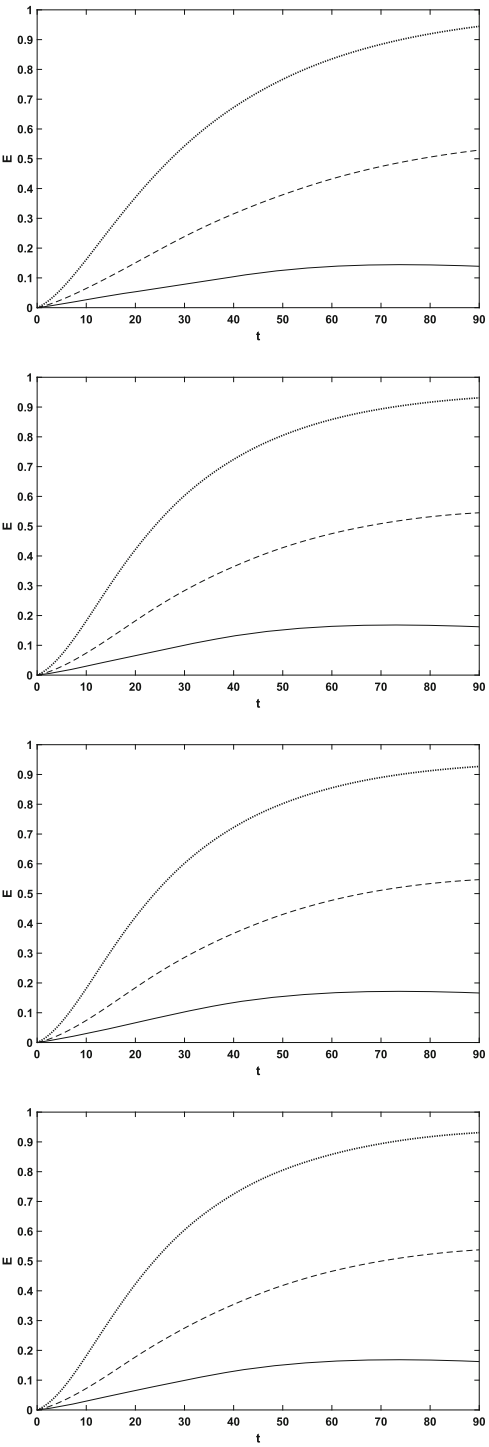

Fig. 14 The time evolution of the energy $\mathbf{E}[\mathbf{F}, \mathbf{f}](t)$ allocated into the energy storage for $a = 3$ and $c = 4$ m/s (first row panel), for $a = 3$ and $c = 10$ m/s (second row panel), for $a = 6$ and $c = 10$ m/s (third row panel), for $a = 2$ and $c = 10$ m/s (fourth row panel panel), for $F = 0.05$ (solid line), for $F = 0.1$ (dashed line) and for $F = 0.2$ (dot line)

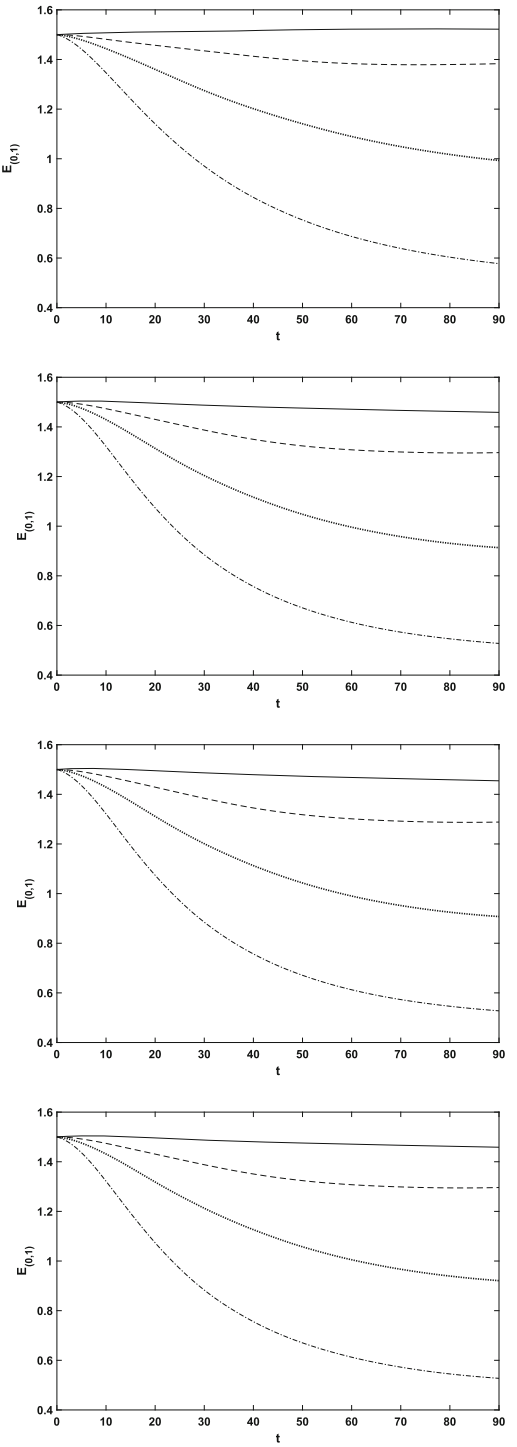

Fig. 15 The time evolution of the global moment $\mathbb{E}^{[\mathbf{F}]}_{(0,1)}[\mathbf{f}](t)$ for $a = 3$ and $c = 4$ m/s (first row panel), for $a = 3$ and $c = 10$ m/s (second row panel), for $a = 6$ and $c = 10$ m/s (third row panel), for $a = 2$ and $c = 10$ m/s (fourth row panel), for $F = 0$ (solid line), for $F = 0.05$ (dashed line), for $F = 0.1$ (dot line) and for $F = 0.2$ (dashed-dot line)

order to model different market trends. In particular, from the modeling point of view, the following scenarios are taken into account:

(a) The fossil fuel price is high: the stochastic term $\Gamma(t)$ takes values in the neighborhood of 0.8.
(b) The fossil fuel price is low: the stochastic term $\Gamma(t)$ takes values in the neighborhood of 0.2.
(c) The fossil fuel price is highly fluctuating: the stochastic term $\Gamma(t)$ takes values in the neighborhood of 0.2 and in the neighborhood of 0.8.

The parameters $(\epsilon_{11}(t), \epsilon_{12}(t), \epsilon_{21}(t), \epsilon_{22}(t))$ of the mathematical model (1) are set as follows:

$$\begin{cases} \epsilon_{11}(t) := (1 - \Gamma(t))\ \epsilon_{11}, \\ \epsilon_{12}(t) := (1 - \Gamma(t))\ \epsilon_{12}, \\ \epsilon_{21}(t) := \Gamma(t)\epsilon_{21}, \\ \epsilon_{22}(t) := \Gamma(t)\epsilon_{22}, \end{cases} \tag{18}$$

where $\epsilon_{lj} \in [0, 1]$, for $l, j \in \{1, 2\}$, is a fixed parameter. The activation of the energy source NR is promoted when the price of the fossil fuel is low ($\epsilon_{11}(t)$ and $\epsilon_{12}(t)$) and the activation of the energy source R is promoted when the price of the fossil fuel is high ($\epsilon_{21}(t)$ and $\epsilon_{22}(t)$).

Bearing all above in mind, the mathematical model (6) now writes:

$$\begin{aligned} \partial_t f_1(t, w) = {} & (1 - \Gamma(t))\,\epsilon_{11}\,(\alpha + \beta)\ f_1(t, w) \int_{D_w} f_1(t, w^*)\,\mathrm{d}w^* \\ & + (1 - \Gamma(t))\,\epsilon_{12}\,\alpha\ f_1(t, w + \lambda_1) \int_{D_w} f_2(t, w^*)\,\mathrm{d}w^* \\ & + (1 - \Gamma(t)\,\epsilon_{21})\ \alpha\ f_2(t, w - \lambda_2) \int_{D_w} f_1(t, w^*)\,\mathrm{d}w^* \\ & + (1 - \Gamma(t)\,\epsilon_{22})\,(\alpha + \beta)\ f_2(t, w) \int_{D_w} f_2(t, w^*)\,\mathrm{d}w^* \\ & - f_1(t, w) \int_{D_w} \big((\alpha + \beta)\ f_1(t, w^*) + \alpha f_2(t, w^*)\big)\,\mathrm{d}w^*, \\ \partial_t f_2(t, w) = {} & (1 - (1 - \Gamma(t))\,\epsilon_{11})\,(\alpha + \beta)\ f_1(t, w) \int_{D_w} f_1(t, w^*)\,\mathrm{d}w^* \\ & + (1 - (1 - \Gamma(t))\,\epsilon_{12})\ \alpha\ f_1(t, w + \lambda_1) \int_{D_w} f_2(t, w^*)\,\mathrm{d}w^* \\ & + \Gamma(t)\,\epsilon_{21}\,\alpha\ f_2(t, w - \lambda_2) \int_{D_w} f_1(t, w^*)\,\mathrm{d}w^* \\ & + \Gamma(t)\,\epsilon_{22}\,(\alpha + \beta)\ f_2(t, w) \int_{D_w} f_2(t, w^*)\,\mathrm{d}w^* \\ & - f_2(t, w) \int_{D_w} \big(\alpha\ f_1(t, w^*) + (\alpha + \beta)\ f_2(t, w^*)\big)\,\mathrm{d}w^*. \end{aligned} \tag{19}$$

The parameters are set as in the previous section: $\alpha = 0.6$, $\beta = 0.1$, $\epsilon_{11} = 0.5 = \epsilon_{22}$, $\epsilon_{12} = 0.3$, $\epsilon_{21} = 0.8$, $\lambda_1 = 0.5$ and $\lambda_2 = 0.6$. In particular, as already mentioned, the choice $\epsilon_{12} < \epsilon_{21}$ ensures the promotion of the virtuous trend in the energy distribution.

The different scenarios can be analyzed by depicting the moments $\mathbb{E}_{(0,0)}[f_1](t)$ and $\mathbb{E}_{(0,0)}[f_2](t)$ (number of customers served by the energy source NR and R, respectively)

and the moments $\mathbb{E}_{(0,1)}[f_1](t)$ and $\mathbb{E}_{(0,0)}[f_2](t)$ (average energy provided by the energy source NR and R respectively).

In the case (a), the market is characterized by a high value of the fossil fuel price, then $\Gamma(t)$ mostly takes high values in the neighborhood of 0.8. As the Fig. 16 shows, the trend is virtuous because most of the customers are supplied by the energy source R, namely $\mathbb{E}_{(0,0)}[f_1](t) < \mathbb{E}_{(0,0)}[f_2](t)$ for all t, and the average energy value provided by the energy source R becomes bigger than the average energy value provided by the energy source NR, namely $\mathbb{E}_{(0,1)}[f_1](t) < \mathbb{E}_{(0,1)}[f_2](t)$ for all t.

In the case (b) the trend in the market is characterized by a low value of the fossil fuel price, $\Gamma(t)$ mostly takes values in the neighborhood of 0.2. As shown in the second and third row panels of the Fig. 17, the trend is not virtuous. The most part of the customers is served with the energy produced by the energy source NR, i.e. $\mathbb{E}_{(0,0)}[f_1](t) > \mathbb{E}_{(0,0)}[f_2](t)$ for all t, and the most part of the energy provided to the customers is produced by the energy source NR, i.e. $\mathbb{E}_{(0,1)}[f_1](t) > \mathbb{E}_{(0,1)}[f_2](t)$ for all t.

In the case (c), the fossil fuel price fluctuates ($\Gamma(t)$ mostly takes values in the neighborhood of 0.2 and 0.8). As the Fig. 18 shows, the model exhibits a virtuous trend.

An important analysis is related to the construction of the energy storage during the fossil fuel price fluctuations. Accordingly the mathematical model (1) rewrites as follows:

$$
\begin{aligned}
&\partial_t f_1(t,w) + F\,\partial_w\left(\left(1-\alpha_{(2,2)}[\mathbf{f}](t)\,w\right) f_1(t,w)\right)\\
&= (1-\Gamma(t))\,\epsilon_{11}\,(\alpha+\beta)\; f_1(t,w)\int_{D_w} f_1(t,w^*)\,\mathrm{d}w^*\\
&\quad + (1-\Gamma(t))\,\epsilon_{12}\,\alpha\, f_1(t,w+\lambda_1)\int_{D_w} f_2(t,w^*)\,\mathrm{d}w^*\\
&\quad + (1-\Gamma(t)\,\epsilon_{21})\;\alpha\, f_2(t,w-\lambda_2)\int_{D_w} f_1(t,w^*)\,\mathrm{d}w^*\\
&\quad + (1-\Gamma(t)\,\epsilon_{22})\,(\alpha+\beta)\; f_2(t,w)\int_{D_w} f_2(t,w^*)\,\mathrm{d}w^*\\
&\quad - f_1(t,w)\int_{D_w}\left((\alpha+\beta)\; f_1(t,w^*)+\alpha f_2(t,w^*)\right)\mathrm{d}w^*,\\
&\partial_t f_2(t,w) + F\,\partial_w\left(\left(1-\alpha_{(2,2)}[\mathbf{f}](t)\,w\right) f_2(t,w)\right)\\
&= (1-(1-\Gamma(t))\,\epsilon_{11})\,(\alpha+\beta)\; f_1(t,w)\int_{D_w} f_1(t,w^*)\,\mathrm{d}w^*\\
&\quad + (1-(1-\Gamma(t))\,\epsilon_{12})\;\alpha\, f_1(t,w+\lambda_1)\int_{D_w} f_2(t,w^*)\,\mathrm{d}w^*\\
&\quad + \Gamma(t)\,\epsilon_{21}\,\alpha\, f_2(t,w-\lambda_2)\int_{D_w} f_1(t,w^*)\,\mathrm{d}w^*\\
&\quad + \Gamma(t)\,\epsilon_{22}\,(\alpha+\beta)\; f_2(t,w)\int_{D_w} f_2(t,w^*)\,\mathrm{d}w^*\\
&\quad - f_2(t,w)\int_{D_w}\left(\alpha\, f_1(t,w^*)+(\alpha+\beta)\; f_2(t,w^*)\right)\mathrm{d}w^*\\
&\quad - f_1(t,w)\int_{D_w}\left((\alpha+\beta)\; f_1(t,w^*)+\alpha f_2(t,w^*)\right)\mathrm{d}w^*,
\end{aligned}
\tag{20}
$$

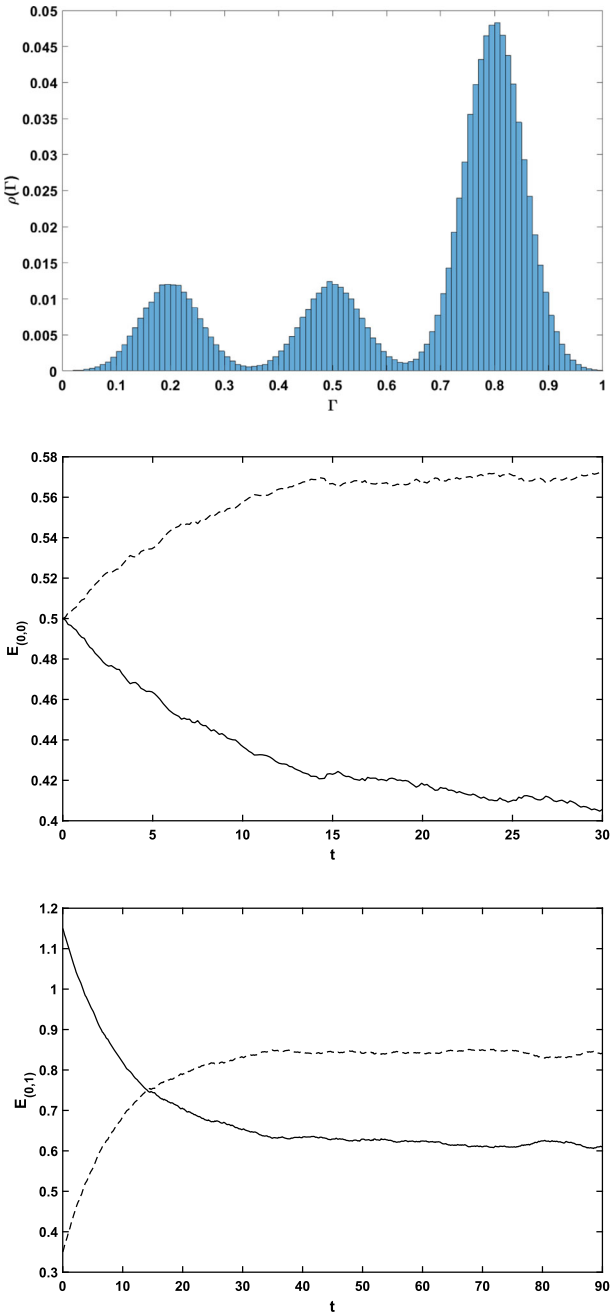

Fig. 16 The distribution $\rho(\Gamma)$ (first row panel), the time evolution of the moments $\mathbb{E}_{(0,0)}[f_1](t)$ related to the energy source NR (second row panel-solid line) and $\mathbb{E}_{(0,0)}[f_2](t)$ related to the energy source R (second row panel-dashed line), the time evolution of the moments $\mathbb{E}_{(0,1)}[f_1](t)$ related to the energy source NR (third row panel-solid line) and $\mathbb{E}_{(0,1)}[f_2](t)$ related to the energy source R (third row panel-dashed line), in the case (a)

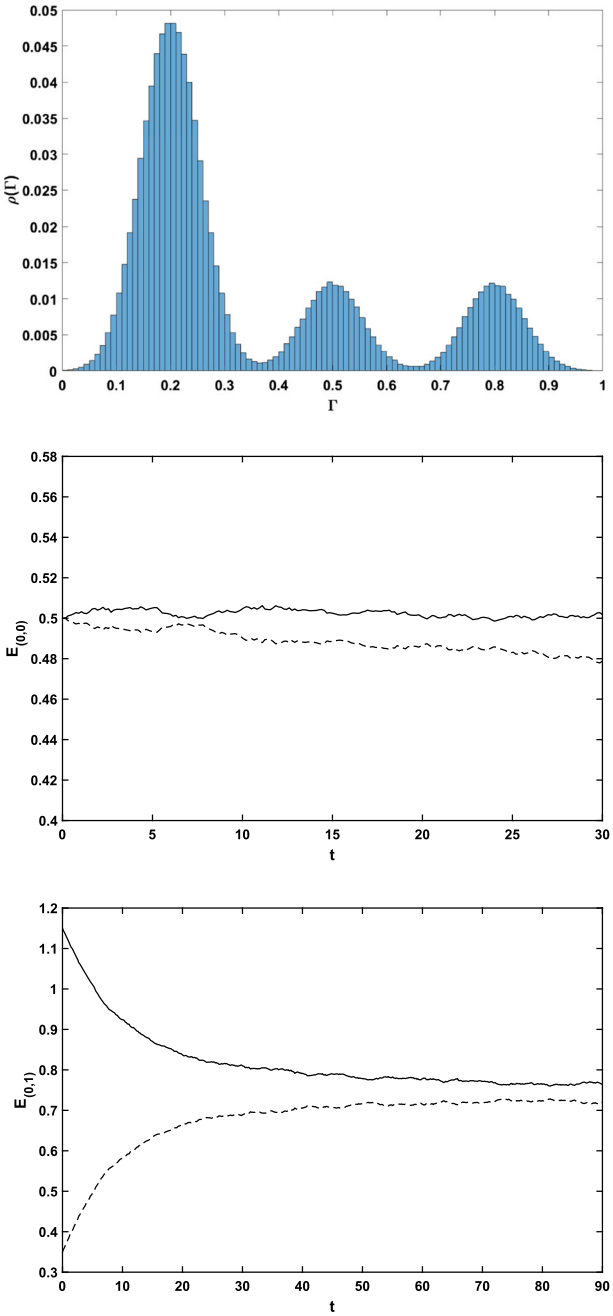

Fig. 17 The distribution $\rho(\Gamma)$ (first row panel), the time evolution of the moments $\mathbb{E}_{(0,0)}[f_1](t)$ related to the energy source NR (second row panel-solid line) and $\mathbb{E}_{(0,0)}[f_2](t)$ related to the energy source R (second row panel-dashed line), the time evolution of the moments $\mathbb{E}_{(0,1)}[f_1](t)$ related to the energy source NR (third row panel-solid line) and $\mathbb{E}_{(0,1)}[f_2](t)$ related to the energy source R (third row panel-dashed line), in the case (b)

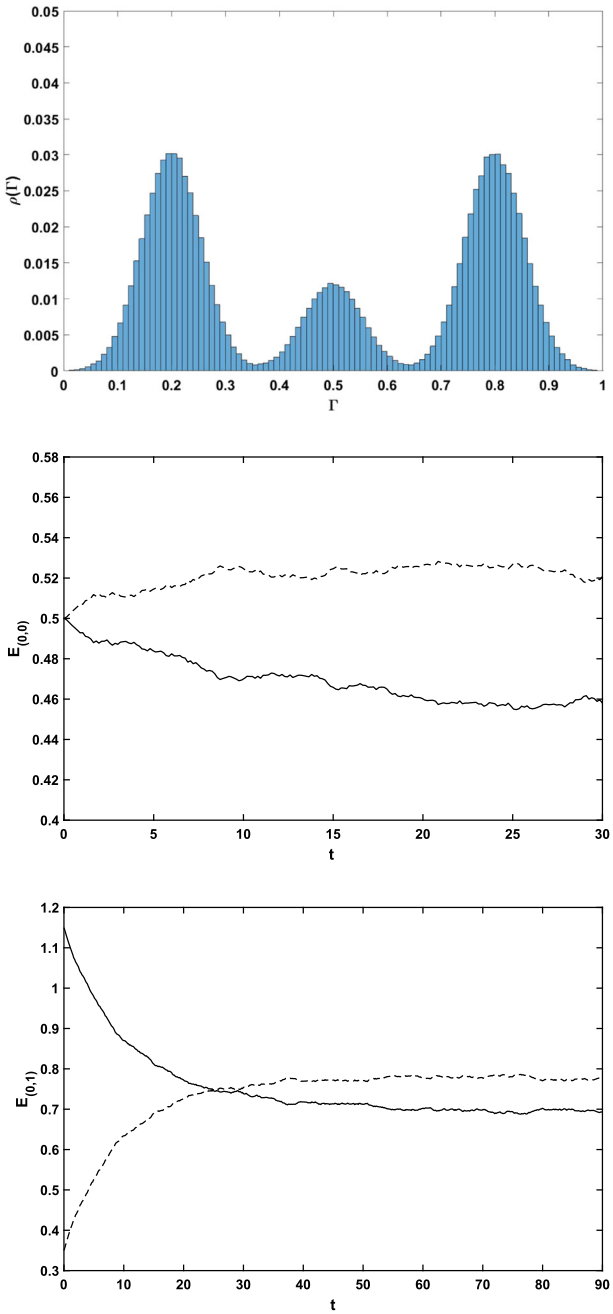

Fig. 18 The distribution $\rho(\Gamma)$ (first row panel), the time evolution of the moments $\mathbb{E}_{(0,0)}[f_1](t)$ related to the energy source NR (second row panel-solid line) and $\mathbb{E}_{(0,0)}[f_2](t)$ related to the energy source R (second row panel-dashed line), the time evolution of the moments $\mathbb{E}_{(0,1)}[f_1](t)$ related to the energy source NR (third row panel-solid line) and $\mathbb{E}_{(0,1)}[f_2](t)$ related to the energy source R (third row panel-dashed line), in the case (c)

where the thermostat term $\alpha_{(2,2)}[\mathbf{f}](t)$ is given by Eq. (2).

Figure 19 shows that the energy $\mathbf{E}[\mathbf{F}, \mathbf{f}](t)$ allocated into the storage increases over time until the achievement of an asymptotic value (maximum amount of energy allocated into the storage). This value increases with the magnitude F, as expected. Consequently, as F increases, less and less energy is directly supplied to the customers: as shown in the Fig. 20, the increase in the magnitude F produces the decrease in the energy value $\mathbb{E}^{[\mathbf{F}]}_{(0,1)}[\mathbf{f}](t)$ provided to the customers. The numerical simulations are carried out for a time interval which ensures that the model describes the allocation of energy into the storage.

It is worth stressing that the construction process of the energy storage is not affected by the trend in the fossil fuel price. The network $\mathcal{N}$ manages the oscillations due to the stochastic term $\Gamma(t)$ and ensures the allocation of the energy $\mathbf{E}[\mathbf{F}, \mathbf{f}](t)$ into the storage.

As already mentioned in the previous sections, a less virtuous scenario produces a slower construction of the storage (compare the first and second row panels of the Fig. 19).

6 Discussions and research perspectives

The present paper has been devoted to the modeling of a solar, a wind and a fossil fuel energy source, within the thermostatted kinetic theory framework proposed in [24]. The representation of the energy sources is realized by means of distribution functions whose time evolution is described by the nonlinear integro-differential system (1). The introduction of an external force field, coupled to a thermostat term, allows to model the construction of the energy storage.

Specifically, in the present paper a network $\mathcal{N}$ composed by a non-renewable and a renewable energy source has been considered. Differently from the model analyzed in [34], in the model (1), time-dependent activation parameters $\epsilon_{ij}(t)$, for $i, j \in \{1, 2\}$, are considered. The parameters aim at modeling the time-dependent efficiency of a specific energy source: the solar energy source is activated according to the solar irradiation, the wind energy source is activated according to the wind speed, the fossil fuel energy source is controlled according to the price of the fossil fuel.

A numerical analysis has been performed to enlighten the effect of the time-dependent activation parameters on the energy production and on the construction process of the energy storage. In particular the activation of the solar energy source is driven by a periodic function $g(t)$, see Eq. (9), which mimics the day–night cycle. The numerical simulations show how the increase in the duration of the night-time interval produces the decrease in the number of customers $\mathbb{E}_{(0,0)}[f_2](t)$ served by the solar energy source and in the energy $\mathbb{E}_{(0,1)}[f_2](t)$ produced by the solar energy source. The activation of the wind energy source is driven by a stochastic term $\Lambda(t)$, see the Eq. (15), which mimics the relation between the wind speed and the energy produced by the turbine (power curve). The wind speed values are generated by means of the two-parameter Weibull distribution. Different scenarios, characterized by different wind conditions, are presented. The model is able to capture the expected dependence of the wind energy production on the wind speed values. Finally, the fossil fuel source is controlled according to a stochastic term $\Gamma(t)$, see Eq. (18), which mimics the price of the fossil fuel price. The fossil fuel price is modeled by means of a probability distribution function. Different price scenarios are presented: the increase in the fossil fuel price implies the decrease in the fossil fuel energy produced $\mathbb{E}_{(0,1)[f_1](t)}$ and in the number of customers $\mathbb{E}_{(0,0)}[f_1](t)$ served by the fossil fuel energy source.

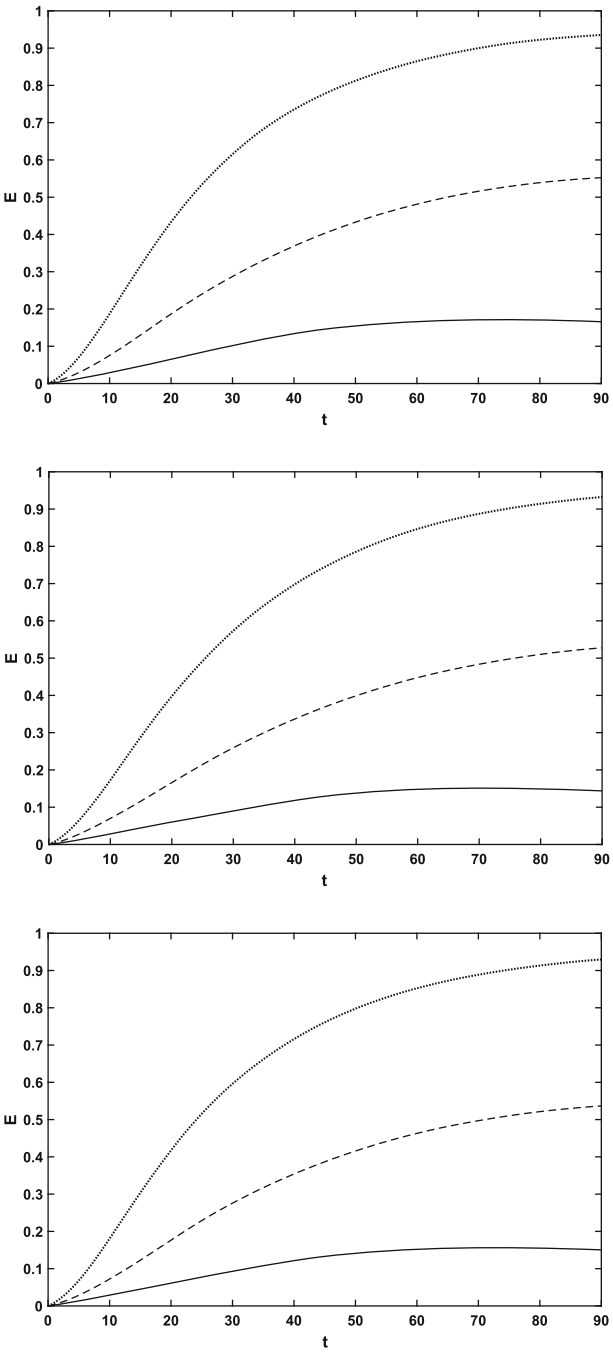

Fig. 19 The time evolution of the energy $\mathbf{E}[\mathbf{F}, \mathbf{f}](t)$ allocated into the energy storage in the case (a) (first row panel), in the case (b) (second row panel), in the case (c) (third row panel), for $F = 0.05$ (solid line), for $F = 0.1$ (dashed line) and for $F = 0.2$ (dot line)

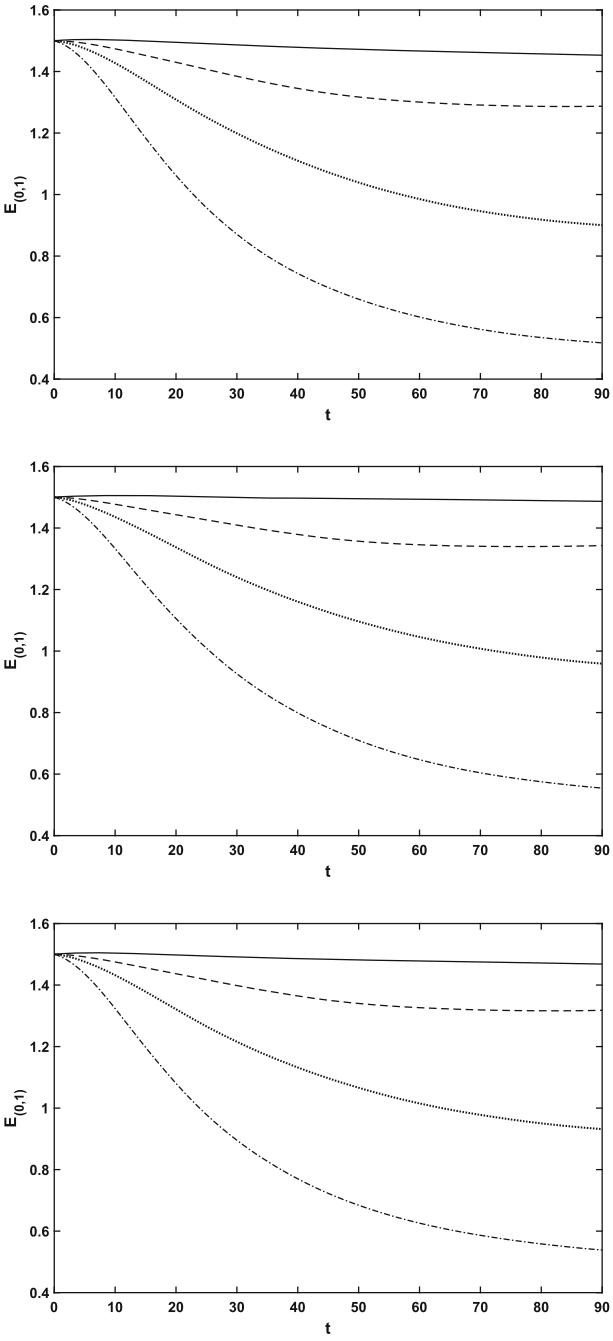

Fig. 20 The time evolution of the global moment $\mathbb{E}^{[\mathbf{F}]}_{(0,1)}[\mathbf{f}](t)$ in the case (a) (first row panel), in the case (b) (second row panel), in the case (c) (third row panel), for $F = 0$ (solid line), for $F = 0.05$ (dashed line), for $F = 0.1$ (dot line) and for $F = 0.2$ (dashed-dot line)

It is worth stressing that the time-dependent activation parameters do not affect the amount of energy $\mathbf{E}[\mathbf{F}, \mathbf{f}](t)$ allocated into the energy storage: the global moment $\mathbb{E}^{[\mathbf{F}]}_{(0,1)}[\mathbf{f}](t)$ does not exhibit the periodic/stochastic fluctuations. The energy $\mathbf{E}[\mathbf{F}, \mathbf{f}](t)$ increases with the increase in the magnitude F of the external force until reaching an asymptotic value (*plateau*) depending on F. The numerical simulations have also revealed that the construction process of the storage is slightly delayed when the trend is not virtuous. This aspect is probably related to the competition between the action of the external force field (shift of the distribution functions towards low values of energy, see [34]) and the growth of the non-renewable distribution function $f_1(t, w)$ at high values of energy. This phenomenon has not been investigated in this paper but can represent a further research direction.

The mathematical model proposed in the present paper can be generalized by increasing the number of sources of the network in order to study the effects of the joint action of the different time-dependent activation parameters on the system. In particular, the interactions of the renewable energy sources can be weighted in order to model their low reliability with respect to the fossil fuel energy sources. The reader interested in the introduction of specific weights into the thermostatted kinetic theory framework is addressed to [48].

A time-dependent external force field can be considered in order to model the control that the network exerts on the construction process of the energy storage [49,50]. The action of the external force can be linked to the achievement of a certain amount of energy allocated into the storage.

The present paper has focused on the construction of the energy storage. However, the role of the energy storage can be reversed in order to model the supply of energy from the storage to the network. Accordingly, the energy storage system can be considered as an external energy source and modeled as a functional subsystem described by a distribution function $f^{\mathbf{S}}(t, w) : [0, +\infty[\times D_w \to \mathbb{R}^+$ (open system). The storage functional subsytem $f^{\mathbf{S}}(t, w)$ can be modeled within the frameworks proposed in [51,52]. The energy storage can be also splitted into different sub-storage systems $f^{\mathbf{S}}_l(t, w)$, for $l \in \{1, 2, \ldots, n\}$, placed in different regions of the network. The modeling of the interactions between the energy storage systems and the energy sources then allows to optimize the allocation and the employment of the storage. The results of this analysis can be compared with other works, e.g. [53], where the optimization methods are addressed to the minimization of the network losses and costs by means of the energy storage system.

Another interesting modeling perspective is the simulation of failures into the network in order to study the vulnerability of the multisource system. This is an important topic which has attracted many researchers, for a complex network approach see [54,55]. The failure processes can be modeled within the thermostatted kinetic theory framework by reducing the ability of a certain source to interact with the others, see [56]. It is worth stressing that this approach allows to model phenomena characterized by different intensity, like brownout and blackout, while the complex network approach relies on the removal of a node of the network and the intensity cannot be directly adjusted [57,58].

The validation of the model (1) requires the tuning of the parameters with empirical data. On the one hand, a validated model allows the researchers to analyze the efficiency of the existing energy source network and to perform a comparison with the results obtained by means of other methods. In particular, the thermostatted kinetic theory model proposed in the present paper provides the control of the produced energy and allows to optimize the network, with respect to environmental and economic aspects, by means of the modeling of the interactions between the energy sources. The Petri Nets approach proposed in [59] has already showed the importance of the interconnections among the energy sources for the

optimization of the energy distribution; however, the introduction of a new parameter in the dynamics implies the definition of a new set of nodes and transitions [60]. The thermostatted kinetic theory framework appears more flexible: The introduction of new parameters can be realized more easily by modifying the existing parameters of the systems. Moreover, the thermostatted kinetic theory approach is based on differential equations which describe the time evolution of the system and more in general provide an analysis on equilibria and asymptotic behavior

It is worth stressing that, to the best of our knowledge, this is the first time that the number of customers is taken into account in the modeling of a energy multisource system which usually focused on the matching between the energy production and demand [61].

On the other hand, the interest in the model validation is the optimization and the design of the future energy multisource systems, with special attention to the role of the renewable energy sources. Indeed, the integration of the renewable energy sources into the energy source network is an important topic that must be taken into account during the conception process of the future networks, even at national scale [62–64]. In particular, the meteorological data will be taken into account as input information for the control of the multisource system in presence of solar and wind energy sources as in [65,66] where the solar and wind conditions of different sites are considered.

A The hybrid thermostatted kinetic theory framework

This appendix deals with the hybrid thermostatted kinetic theory framework for the modeling of a network $\mathcal{N}$ composed of $\mathbf{N} = 2$ energy sources: a non-renewable energy source NR and a renewable energy source R. The energy storage is also taken into account.

A discrete quality parameter $u \in [0, 1]$ identifies the energy sources and specifically the energy source NR is associated with $u_1 = 1/3$ (low quality), while the energy source R is associated with $u_2 = 2/3$ (high quality). Each energy source is a functional subsystem and is described by means of the distribution function $f_i(t, w) : [0, +\infty[\times D_w \to \mathbb{R}^+$, for $i \in \{1, 2\}$, over the microscopic state $w \in D_w \subset \mathbb{R}^+$ which models the continuous energy variable. Accordingly, $f_i(t, w)dw$ represents the number of customers served at time t with an energy value $w \in [w, w + dw]$ which is produced by the energy source u_i, for $i \in \{1, 2\}$.

The introduction of an external positive force field $\mathbf{F} = (F_1, F_2) \in (\mathbb{R}^+)^2$, acting on each functional subsystem, models the construction of the energy storage. The external force takes a certain amount of the energy produced by the sources and allocates it into the energy storage. From the mathematical point of view, the external force field $\mathbf{F}$ moves the system far from the equilibrium. Therefore, a thermostat term $\alpha_{(2,2)}[\mathbf{F}, \mathbf{f}](t)$, where $\mathbf{f} = (f_1(t, w), f_2(t, w))$ is also considered in order to control the global activation energy of the system and allows the existence of a nonequilibrium stationary state.

The macroscopic quantities are represented by the moments of the distribution function. Specifically the global (p, q)-th order moment writes:

$$\mathbb{E}^{[\mathbf{F}]}_{(p,q)}[\mathbf{f}](t) = \sum_{i=1}^{2} u_i^p \int_{D_w} w^q \, f_i(t, w) \, \mathrm{d}w, \quad \forall \, p, q \in \mathbb{N}. \tag{21}$$

In particular, it is assumed that $\mathbb{E}^{[\mathbf{F}]}_{(0,0)}[\mathbf{f}](t) = 1$ for $t \in [0, +\infty[$ (normalization condition). In the case $\mathbf{F} = \mathbf{0}$, the notation $\mathbb{E}^{[\mathbf{F}=\mathbf{0}]}_{(p,q)}[\mathbf{f}](t)$ simplifies into $\mathbb{E}_{(p,q)}[\mathbf{f}](t)$.

The energy sources interact via the network $\mathcal{N}$ thus modifying their microscopic state. The time evolution of the distribution function $f_i(t, w)$ is given by balancing the inlet and outlet flows into the elementary volume $[w, w + dw]$:

$$\partial_t f_i(t, w) + \partial_w \left(\left(F_i - \alpha_{(2,2)}[\mathbf{F}, \mathbf{f}](t)\, w \right) f_i(t, w) \right) = J_i[\mathbf{f}](t, w), \quad i \in \{1, 2\}, \tag{22}$$

where $J_i[\mathbf{f}](t, w) = G_i[\mathbf{f}](t, w) - L_i[\mathbf{f}](t, w)$, for $i \in \{1, 2\}$, being $G_i[\mathbf{f}](t, w)$ and $L_i[\mathbf{f}](t, w)$ the gain term and the loss term, respectively, that write as follows:

$$G_i[\mathbf{f}](t, w) = \sum_{l=1}^{2} \sum_{j=1}^{2} \int_{D_w \times D_w} \eta_{lj} \left(w_*, w^* \right) \mathcal{B}^i_{lj}\, \mathcal{A}_{lj} \left(w_*, w^*; w \right) \times f_l(t, w_*)\, f_j(t, w^*)\, \mathrm{d}w_*\, \mathrm{d}w^*, \tag{23}$$

$$L_i[\mathbf{f}](t, w) = f_i(t, w) \sum_{j=1}^{2} \int_{D_w} \eta_{ij} \left(w, w^* \right) f_j(t, w^*)\, dw^*, \tag{24}$$

and the functional parameters have the following meaning:

- $\eta_{lj}\,(w_*, w^*) : D_w \times D_w \to \mathbb{R}^+$ denotes the interaction rate between the energy source u_l, with the energy value w_*, and the energy source u_j, with the energy value w^*.
- $\mathcal{A}_{lj}\,(w_*, w^*; w) : D_w \times D_w \times D_w \to \mathbb{R}^+$ denotes the probability of the evolution of the energy value w_* of the source u_l into the energy value w, after the interaction with the source u_j with the energy value w^*. Then one has

$$\int_{D_w} \mathcal{A}_{lj} \left(w_*, w^*; w \right) \mathrm{d}w = 1, \quad \forall\, w_*, w^* \in D_w. \tag{25}$$

- $\mathcal{B}^i_{lj}$ denotes the probability of the activation of the energy source u_i after the interaction between the energy source u_l and the energy source u_j. Then one has

$$\sum_{i=1}^{2} \mathcal{B}^i_{lj} = 1, \quad \forall l, j \in \{1, 2\}. \tag{26}$$

The thermostat term $\alpha_{(2,2)}[\mathbf{F}, \mathbf{f}](t)$ reads:

$$\alpha_{(2,2)}[\mathbf{F}, \mathbf{f}](t) = \frac{\sum_{j=1}^{2} F_j u_j^2 \int_{D_w} w\, f_j(t, w)\, \mathrm{d}w}{\mathbb{E}^{[\mathbf{F}]}_{(2,2)}[\mathbf{f}](t)}, \tag{27}$$

and controls the global $(2, 2)$-order moment $\mathbb{E}^{[\mathbf{F}]}_{(2,2)}[\mathbf{f}](t)$.

The model analyzed in this work is derived from the framework (22) by considering the following assumptions:

- The interaction rate $\eta_{lj}\,(w_*, w^*) : D_w \times D_w \to \mathbb{R}^+$ is modeled as follows:

$$\eta_{lj}(w_*, w^*) = \alpha + \beta \delta_{lj}, \quad \alpha, \beta \in \mathbb{R}^+, \tag{28}$$

  where δ_{lj} denotes the delta of Kronecker. In particular it is assumed that the autointeraction rates are greater than the interaction rates between two different energy sources, i.e. $\eta_{ll} > \eta_{lj}$.

– The probability $\mathcal{A}_{lj}\ (w_*, w^*; w) : D_w \times D_w \times D_w \to \mathbb{R}^+$ is modeled as follows:

$$\mathcal{A}_{lj}(w_*, w^*; w) = \delta(w - d_{lj}(w_*, w^*)), \tag{29}$$

where $\delta(\cdot)$ denotes the delta of Dirac and

$$d_{lj}(w_*, w^*) = \begin{cases} w_* - \lambda_1 & \text{if } \ l = 1 \ \text{ and } \ j = 2, \\ w_* + \lambda_2 & \text{if } \ l = 2 \ \text{ and } \ j = 1, \\ w_* & \text{if } \ l = j, \end{cases} \tag{30}$$

and $\lambda_1, \lambda_2 \in [0, 1]$. The choice of the definition (30) relies on the following assumptions: the energy source NR should reduce its energy value, the energy source R should increase its energy value, the autointeraction does not modify the energy value of an energy source.

– The probability $\mathcal{B}^i_{lj}$ is modeled as follows:

$$\mathcal{B}^i_{lj} = \begin{cases} \epsilon_{lj}(t) & \text{if } \ i = l, \\ 1 - \epsilon_{lj}(t) & \text{if } \ i \neq l, \end{cases} \tag{31}$$

where $\epsilon_{lj}(t) : [0, +\infty[\to [0, 1]$, for $l, j \in \{1, 2\}$. Specifically, $\epsilon_{1j}(t)$ and $\epsilon_{2j}(t)$, for $j \in \{1, 2\}$, denotes the probability of the activation of the energy source NR and R, respectively.

References

1. B.D. Solomon, K. Krishna, The coming sustainable energy transition: history, strategies, and outlook. Energy Policy **39**, 7422–7431 (2011)
2. A.N. Menagaki, K.P. Tsagarakis, Rich enough to go renewable, but too early to leave fossil energy? Renew. Sustain. Energy Rev. **41**, 1465–1477 (2015)
3. B.K. Sovacool, How long will it take? Conceptualizing the temporal dynamics of energy transitions. Energy Res. Soc. Sci. **13**, 202–215 (2016)
4. S. Bolwig, G. Bazbauers, A. Klitkou, P.D. Lund, A. Blumberga, A. Grasvelsins, D. Blumberga, Review of modelling energy transitions pathways with application to energy system flexibility. Renew. Sustain. Energy Rev. **101**, 440–452 (2019)
5. M. Talaat, M.A. Farahat, M.H. Elkholy, Renewable power integration: experimental and simulation study to investigate the ability of integrating wave, solar and wind energies. Energy **170**, 668–682 (2019)
6. A.S. Dagoumas, N.E. Koltsaklis, Review of models for integrating renewable energy in the generation expansion planning. Appl. Energy **242**, 1573–1587 (2019)
7. F. Romanelli, Strategies for the integration of intermittent renewable energy sources in the electrical system. Eur. Phys. J. Plus **131**, 53 (2016)
8. G. Notton, M.-L. Nivet, C. Voyant, C. Paoli, C. Darras, F. Motte, A. Fouilloy, Intermittent and stochastic character of renewable energy sources: consequences, cost of intermittence and benefit of forecasting. Renew. Sustain. Energy Rev. **87**, 96–105 (2018)
9. A. Ghoshray, B. Johnson, Trends in world energy prices. Energy Econ. **32**, 1147–1156 (2010)
10. G. Filatrella, A.H. Nielsen, N.F. Pedersen, Analysis of a power grid using a Kuramoto-like model. Eur. Phys. J. B **61**, 485–491 (2008)
11. R. Carareto, M.S. Baptista, C. Grebogi, Natural synchronization in power-grids with anti-correlated units. Commun. Nonlinear Sci. Numer. Simul. **18**, 1035–1046 (2013)
12. A. Sciré, I. Tuval, V.M. Eguíluz, Dynamic modeling of the electric transportation network. Europhys. Lett. **71**, 318–324 (2005)
13. G.A. Pagani, M. Aiello, The power grid as a complex network: a survey. Phys. A **392**, 2688–2700 (2013)
14. R. Baños, F. Manzano-Agugliaro, F.G. Montoya, C. Gil, A. Alcayde, J. Gómez, Optimization methods applied to renewable and sustainable energy: a review. Renew. Sustain. Energy Rev. **15**, 1753–1766 (2011)
15. K.-H. Chang, G. Lin, Optimal design of hybrid renewable energy systems using simulation optimization. Simul. Model. Pract. Theory **52**, 40–51 (2015)
16. P.H.J. Nardelli, N. Rubido, C. Wang, M.S. Baptista, C. Pomalaza-Raez, P. Cardieri, M. Latva-aho, Models for the modern power grid. Eur. Phys. J. Spec. Topics **223**, 2423–2437 (2014)

17. X. Fang, S. Misra, G. Xue, D. Yang, Smart grid—the new and improved power grid: a survey. IEEE Commun. Surv. Tutor. **14**, 944–980 (2012)
18. M.L. Tuballa, M.L. Abundo, A review on the development of smart grid technologies. Renew. Sustain. Energy Rev. **59**, 710–725 (2016)
19. S. Bigerna, C.A. Bollino, S. Micheli, Socio-economic acceptability for smart grid development—a comprehensive review. J. Clean. Prod. **131**, 399–409 (2016)
20. M.S. Hossain, N.A. Madlool, N.A. Rahim, J. Selvaraj, A.K. Pandey, A.F. Khan, Role of smart grid in renewable energy: an overview. Renew. Sustain. Energy Rev. **60**, 1168–1184 (2016)
21. M. Ourahou, W. Ayrir, B. El Hassouni, A. Haddi, Review on smart grid control and reliability in presence of renewable energies: challenges and prospects. Math. Comput. Simul. (2018). https://doi.org/10.1016/j.matcom.2018.11.009
22. S. Mei, X. Zhang, M. Cao, *Power Grid Complexity* (Springer, Berlin, 2011)
23. C. Petermann, S.B. Amor, A. Bui, A complex system approach for a reliable smart grid modeling. Front. Artif. Intell. Appl. Adv. Knowl. Based Intell. Inf. Eng. Syst. **243**, 149–158 (2012)
24. M. Dalla Via, C. Bianca, I. El Abbassi, A.-M. Darcherif, A hybrid thermostatted kinetic framework for the modeling of a hybrid multisource system with storage, under review
25. C. Bianca, An existence and uniqueness theorem to the cauchy problem for thermostatted-KTAP models. Int. J. Math. Anal. **6**, 813–824 (2012)
26. C. Bianca, J. Riposo, Mimic therapeutic actions against keloid by thermostatted kinetic theory methods. Eur. Phys. J. Plus **130**, 159 (2015)
27. C. Bianca, L. Brézin, Modeling the antigen recognition by B-cell and Tcell receptors through thermostatted kinetic theory methods. Int. J. Biomath. **10**, 1750072 (2017)
28. C. Bianca, C. Mogno, A thermostatted kinetic theory model for event-driven pedestrian dynamics. Eur. Phys. J. Plus **133**, 213 (2018)
29. W.G. Hoover, A.J.C. Ladd, B. Moran, High-strain-rate plastic flow studied via nonequilibrium molecular dynamics. Phys. Rev. Lett. **48**, 1818–1820 (1982)
30. D.J. Evans, W.G. Hoover, B.H. Failor, B. Moran, A.J.C. Ladd, Nonequilibrium molecular dynamics via Gauss's principle of least constraint. Phys. Rev. A **28**, 1016–1021 (1983)
31. G.P. Morriss, C.P. Dettmann, Thermostats: analysis and application. Chaos **8**, 321–336 (1998)
32. O.G. Jepps, L. Rondoni, Deterministic thermostats, theories of nonequilibrium systems and parallels with the ergodic condition. J. Phys. A Math. Theor. **43**, 133001 (2010)
33. R.B. Myerson, *Game Theory: Analysis of Conflict* (Harvard University Press, Cambridge, 1997)
34. M.D. Via, C. Bianca, I. El Abbassi, A.-M. Darcherif, A thermostatted kinetic theory model for a hybrid multisource system with storage. Appl. Math. Model. **78**, 232–248 (2020)
35. P.J. Davis, P. Rabinowitz, *Methods of Numerical Integration* (Academic Press, London, 1984)
36. A. Veeraragavan, L. Montgomery, A. Datas, Night time performance of a storage integrated solar thermophotovoltaic (SISTPV) system. Sol. Energy **108**, 377–389 (2014)
37. M.S. Yousef, A.K.A. Rahman, S. Ookawara, Performance investigation of low—concentration photovoltaic systems under hot and arid conditions: experimental and numerical results. Energy Convers. Manag. **128**, 82–94 (2016)
38. G. Li, Q. Xuan, X. Zhao, G. Pei, J. Ji, Y. Su, A novel concentrating photovoltaic/daylighting control system: optical simulation and preliminary experimental analysis. Appl. Energy **228**, 1362–1372 (2018)
39. A. Kusiak, H. Zheng, Z. Song, On-line monitoring of power curves. Renew. Energy **34**, 1487–1493 (2009)
40. M. Lydia, S.S. Kumar, A.I. Selvakumar, G.E.P. Kumar, A comprehensive review on wind turbine power curve modeling techniques. Renew. Sustain. Energy Rev. **30**, 452–460 (2014)
41. G.A.M. van Kuik, The Lanchester–Betz–Joukowsky limit. Wind Energy **10**, 289–291 (2007)
42. H. Jiang, Y. Li, Z. Cheng, Performances of ideal wind turbine. Renew. Energy **83**, 658–662 (2015)
43. P. Wais, A review of Weibull functions in wind sector. Renew. Sustain. Energy Rev. **70**, 1099–1107 (2017)
44. https://www.meteoblue.com. Accessed 25 Apr 2019
45. C.N. Nwafor, A.A. Oyedele, Simulation and hedging oil price with geometric Brownian Motion and single-step binomial price model. Eur. J. Bus. Manag. **9**, 68–81 (2017)
46. N. Meade, Oil prices—Brownian motion or mean reversion? A study using a one year ahead density forecast criterion. Energy Econ. **32**, 1485–1498 (2010)
47. S. Mirkhani, Y. Saboohi, Stochastic modeling of the energy supply system with uncertain fuel price—a case of emerging technologies for distributed power generation. Appl. Energy **93**, 668–674 (2012)
48. C. Bianca, M. Menale, On the interaction domain reconstruction in the weighted thermostatted kinetic framework. Eur. Phys. J. Plus **134**, 143 (2019)
49. Y. Yang, S. Bremmer, C. Menictas, M. Kay, Battery energy storage system size determination in renewable energy systems: a review. Renew. Sustain. Energy Rev. **91**, 109–125 (2018)

50. L.A. Wong, V.K. Ramachandaramurthy, P. Taylor, J.B. Ekanayake, S.L. Walker, S. Padmanaban, Review on the optimal placement, sizing and control of an energy storage system in the distribution network. J. Energy Storage **21**, 489–504 (2019)
51. I. Brazzoli, From the discrete kinetic theory to modelling open systems of active particles. Appl. Math. Lett. **21**, 155–160 (2008)
52. C. Bianca, On the modelling of space dynamics in the kinetic theory for active particles. Math. Comput. Modell. **51**, 72–83 (2010)
53. H. Mehrjerdi, R. Hemmati, E. Farrokhi, Nonlinear stochastic modeling for optimal dispatch of distributed energy resources in active distribution grids including reactive power. Simul. Model. Pract. Theory **94**, 1–13 (2019)
54. S. Arianos, E. Bompard, A. Carbone, F. Xue, Power grid vulnerability: a complex network approach. Chaos Interdiscip. J. Nonlinear Sci. **19**, 013119 (2009)
55. Y. Dai, G. Chen, Z. Dong, Y. Xue, D.J. Hill, Y. Zhao, An improved framework for power grid vulnerability analysis considering critical system features. Phys. A **395**, 405–415 (2014)
56. C. Bianca, Modeling complex systems with particles refuge by thermostatted kinetic theory methods. Abstr. Appl. Anal. **2013**, 152174 (2013)
57. P. Cruciti, V. Latora, M. Marchiori, A topological analysis of the Italian electric power grid. Phys. A **338**, 92–97 (2004)
58. R. Albert, I. Albert, G.L. Nakarado, Structural vulnerability of the North American power grid. Phys. Rev. E **69**, 025103 (2004)
59. M.A.M. Mouhammad, I. El Abbassi, A.-M. Darcherif, M. El Ganaoui, New robust energy management model for interconnected power networks using Petri Nets approach. Smart Grid Renew. Energy **7**, 46–65 (2016)
60. B.C. Wang, M. Sechilariu, F. Locment, Power flow Petri Net modelling for building integrated multi-source power system with smart grid interaction. Math. Comput. Simual. **91**, 119–133 (2013)
61. A. Hooshmand, H.A. Malki, J. Mohammadpour, Power flow management of microgrid networks using model predictive control. Comput. Math. Appl. **64**, 869–876 (2012)
62. P.-F. Bach, Towards 50% wind electricity in Denmark: dilemmas and challenges. Eur. Phys. J. Plus **131**, 161 (2016)
63. A. Coester, M.W. Hofkes, E. Papyrakis, An optimal mix of conventional power systems in the presence of renewable energy: a new design for the German electricity market. Energy Policy **116**, 312–322 (2018)
64. R.G. Calvet, J.M.M. Duart, S.S. Calle, Present state and perspectives of variable renewable energies in Spain. Eur. Phys. J. Plus **133**, 126 (2018)
65. S. Diaf, G. Notton, M. Belhamel, M. Haddadi, A. Louche, Design and techno-economical optimization for hybrid PV/wind system under various meteorological conditions. Appl. Energy **85**, 968–987 (2008)
66. M. Zaibi, G. Champenois, X. Roboam, J. Belhadj, B. Sareni, Smart power management of a hybrid photovoltaic/wind stand-alone system coupling battery storage and hydraulic network. Math. Comput. Simul. **146**, 210–228 (2018)